SERI/PR-8136-1-T12
(DE82014517)

DEVELOPMENT OF HIGH EFFICIENCY CASCADE SOLAR CELLS

Technical Progress Report No. 5

By
M. L. Timmons
S. M. Bedair
M. F. Lamorte
J. A. Hutchby
M. Simons

January 1982

Work Performed Under Contract No. AC02-77CH00178

Solar Energy Research Institute
Golden, Colorado

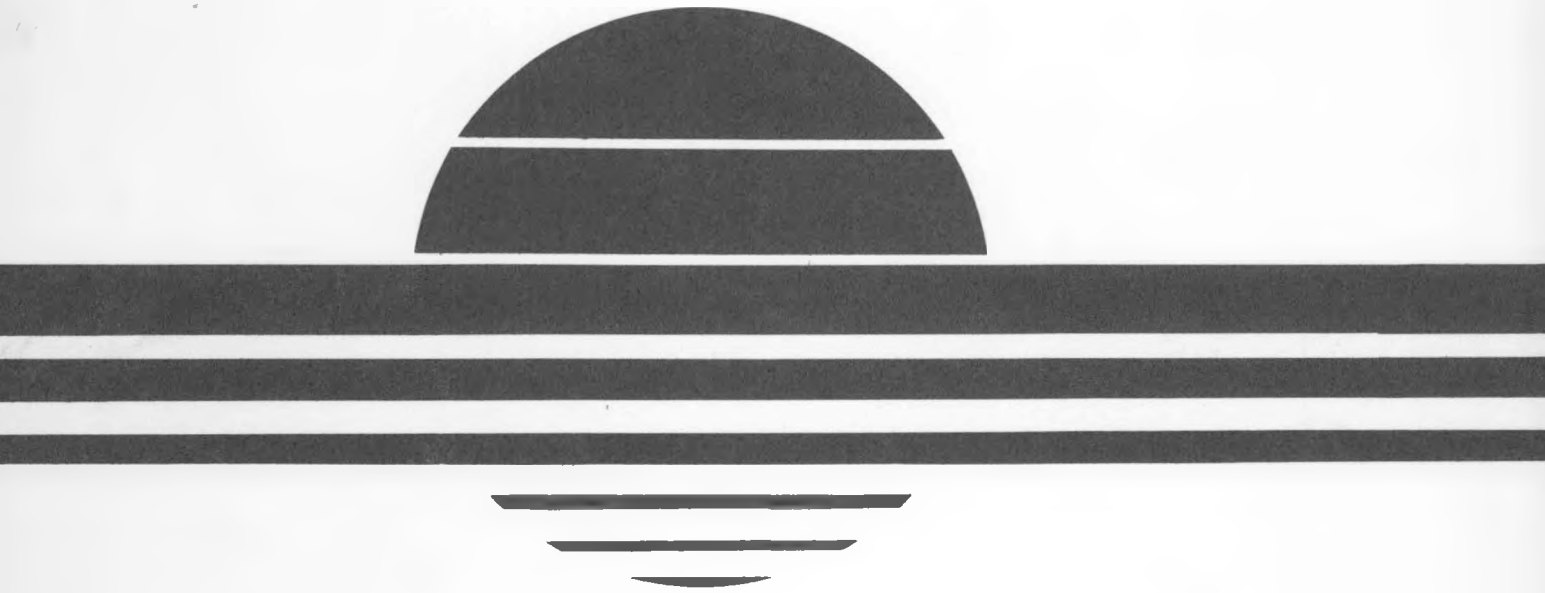

U.S. Department of Energy

Solar Energy

SERI/PR-8136-1-T12
(DE82014517)
Distribution Category UC-63e

TECHNICAL PROGRESS REPORT NO. 5

DEVELOPMENT OF HIGH EFFICIENCY CASCADE SOLAR CELLS

by

M. L. Timmons, S. M. Bedair, M. F. Lamorte, J. A. Hutchby, and M. Simons

January 1982

Contract XM-9-8136-1 under DOE EG-77-C-01-4042

RTI Project 41U-1846

Solar Energy Research Institute

Golden, Colorado

TABLE OF CONTENTS

Page

List of Figures. iv

List of Tables vi

1.0 Introduction. 1

2.0 GaAlAsSb/GaAsSb Cell Development. 4

2.1 Bottom Cell Development. 6
2.2 Top Cell Development 12
2.3 Tunnel Junction Development. 13
2.4 Cascade Cell Growth Experiments. 14
2.5 OM-CVD Growth of GaAsSb. 17
2.6 Conclusions. 27

3.0 AlGaAs/GaAs Cell Development. 28

4.0 Computer Modeling of AlGaAs/GaAs Cell for High Solar Concentration 35

4.1 Analytical Technique 35
4.2 Results and Discussion 36

References 48

LIST OF FIGURES

Figure No.	Title	Page
2.1	GaAlAsSb/GaAsSb Cascade Cell.	5
2.2	Demonstration of the Effect of Increasing the Number of Constant-Composition Layers Between a GaAsSb Junction and Step-Graded Layers	7
2.3	GaAsSb p-n Junction (top two layers) Grown on 48 Constant-Composition and 6 Step-Graded Layers	8
2.4	I-V Characteristic of GaAsSb p-n Junction Grown on 16 Constant-Composition and 6 Step-Graded Layers. . . .	9
2.5	Quantum Efficiency of GaAsSb p-n Junction Grown on 14 Constant-Composition and 6 Step-Graded Layers. . . .	10
2.6	Indication of the Etch Pit Density of a Surface of a GaAsSb p-n Junction Grown on 24 Constant-Composition Layers and 6 Step-Graded Layers	11
2.7	Indication of EPD in the Surface of an AlGaAsSb p-n Junction Grown on 3 Step-Graded Layers and a (111)A GaAs Substrate (440×)	13
2.8	I-V Characteristic of 1.7 eV AlGaAsSb Tunnel Diode. . .	15
2.9	Forward I-V Characteristic of AlGaAsSb Tunnel Junction Using Be as the p-type Dopant.	15
2.10	I-V Curve of Cascade Structure Grown with Ge-doped (abrupt) Junction	16
2.11	Surface Morphology of $GaAs_{0.87}Sb_{0.13}$ Layer Grown on (100) GaAs.	18
2.12	Full-width-at-half-maximum vs Bandgap of OMCVD-Grown GaAsSb.	19
2.13	Cleaved, Stained Cross-section of OMCVD-grown, Multilayered Structure.	21
2.14	Photomicrographs of GaAsSb Layers Grown Simultaneously on (100)- and (111)-GaAs Substrates	22
2.15	Etch Pits for (111)- and (100)-GaAsSb Surfaces.	23
2.16	Etch Pits of Typical (100)-GaAsSb Layer	25
2.17	Effect of Etching on (111)-GaAsSb Layers.	26

LIST OF FIGURES (con't.)

Figure No.	Title	Page
3.1	GaAlAs/GaAs Cascade Cell.	29
3.2	V-I Characteristic for AlGaAs/GaAs Cascade Structure. .	32
3.3	Quantum Efficiency Measured on Cascade Solar Cell Sample R-239-C (3-4) Without AR Coating	33
4.1	Cross Section of AlGaAs/GaAs Cascade Solar Cell Used in the Computer Modeling Study.	37
4.2	Conversion Efficiency vs Temperature: a) 1 sun; b) 500 suns	38
4.3	Voltage at the Maximum Power Point vs Temperature: a) 1 sun; b) 500 suns	42
4.4	Conversion Efficiency vs Solar Concentration at 300 K and 400 K for the Cascade and its Component Cells . . .	44
4.5	Photovoltage at the Maximum Power Point vs Solar Concentration at 300 K and 400 K for the Cascade and its Component Cells	45
4.6	Cascade Cell Photocurrent, Top and Bottom Cell Current Densities vs Solar Concentration for 300 K and 400 K. .	46
4.7	Dark Current vs Temperature: a) 1 sun; b) 500 suns . .	47

LIST OF TABLES

Table No.	Title	Page
4.1	Summary Listing of Conversion Efficiencies for 1 sun and 500 suns and for 300 K and 400 K.	39
4.2	Summary Listing of Photovoltages for 1 sun and 500 suns and for 300 K and 400 K.	39
4.3	Partial Listing of the Normalized Efficiency Temperature Coefficiency for Single- and Two-Junction Cascade Solar Cells.	40

Technical Progress Report No. 5

DEVELOPMENT OF HIGH EFFICIENCY CASCADE SOLAR CELLS

Contract XM-9-8136 Under DOE-EG-77-C-01-4042

1.0 Introduction

This report summarizes the work conducted under the present contract during the six month period from July 1, 1981 to December 31, 1981.

The basic objective of this work is to develop the technology required to fabricate a two-junction cascade solar cell with a conversion efficiency of 30 percent or more under AM1.5 multisun illumination. Intermediate objectives include improving the performance of previously demonstrated AlGaAsSb/GaAsSb and AlGaAs/GaAs experimental cascade solar cell structures and demonstration of a packaged cascade solar cell assembly having a total area of at least 0.5 cm^2 and an efficiency of 25 percent.

Work conducted at RTI previously under contract to SERI has involved both computer modeling and experimental studies of two-junction cascade cells of various bandgap configurations and III-V materials combinations [Ref. 1,2]. In addition to the successful fabrication of demonstration cells in AlGaAs/GaAs and AlGaAsSb/GaAsSb, this work has involved studies in GaAlAs/GaInAs, GaAlAs/GaAsSb and GaInP/GaInAs materials systems. All of the experimental cells have been prepared by standard liquid phase epitaxy (LPE) using a multiple well, horizontal slider graphite boat; related materials studies have also been conducted (and are continuing) using organometallic-chemical vapor deposition (OM-CVD) growth techniques.

The present experimental work is focusing principally on the GaAlAsSb/ GaAsSb cascade cell, which is of particular interest since it

offers the optimum bandgap combination of 1.8/1.2 eV for maximum efficiency in high temperature concentrator applications. Computer modeling studies have shown that a 1.8/1.2 eV cell should be capable of achieving an AM1, 1 sun efficiency (active area) of about 33% at 300 K and 20.5% at 475 K [3]. At 1000 suns (AM1.5), this cell is predicted to have an active area efficiency somewhat greater than 26% at 475 K.

The major problem experienced thus far in the development of the AlGaAsSb/GaAsSb cell has been the relatively low open circuit voltages (V_{oc}) that have been characteristic of both top and bottom cell junctions. Addressing this problem continues to be a major objective of the continued development of this cell.

The AlGaAs/GaAs cell, whose experimental development is being supported principally under Air Force contract, is being retained as a backup to the antimonide cell. Although the AlGaAs/GaAs cell is not capable of achieving the optimum 1.8/1.2 eV bandgap combination, it avoids problems associated with lattice mismatch with the GaAs substrate and offers a more proven materials technology. Computer analysis of this cell (this report) shows that a 1.92/1.43 eV bandgap combination is capable of achieving an active area efficiency of about 27 percent at AM1.5, 300 K, 1 sun. At 500 suns this cell is predicted to have efficiency values of about 30 percent at 300 K and 20 percent at 475 K.

Experimental AlGaAs/GaAs cells without AR coatings have exhibited measured efficiency values of about 16 percent at AM1.5, 1 sun. This development effort has been focusing on performance improvement through improved tunnel junction performance, better ohmic contacts, and an optimized AR coating and on fabricating larger area cells.

Section 2.0 of this report highlights the experimental work conducted during the report period on both AlGaAsSb/GaAsSb and AlGaAs/GaAs cells while Section 3.0 presents the results of computer modeling studies of AlGaAs/GaAs cell performance at high temperatures and high solar concentrations.

2.0 GaAlAsSb/GaAsSb Cell Development

The objective of this research is the development of a GaAlAsSb/GaAsSb cascade cell consisting of a ≃ 1.2 eV GaAsSb bottom cell and a ≃ 1.8 eV AlGaAsSb connecting junction, top cell, and window layer as depicted in Figure 2.1. While the number of active layers required to realize this structure can be as small as five (with diffused junctions), several additional step graded layers (or a continuously graded layer) are needed to compensate for the lattice mismatch (≃ 0.8%) between the bottom cell and the GaAs substrate.

The performance of experimental solar cell structures has been adversely affected by low open circuit voltages that have characterized both top and bottom cells and by interference from the tunnel junction which must provide a good ohmic contact between the two cells. The low V_{oc} problem is believed to stem in part from the lattice mismatch with the substrate while poor tunnel junction performance is attributed to the difficulty in achieving and maintaining an abrupt doping profile between n^+ and p^+ regions.

Efforts during this reporting period have focused principally on improving tunnel junction performance and addressing the lattice mismatch problem through 1) the use of multiple, constant composition LPE layers between substrate and bottom cell and 2) the development of OM-CVD techniques to grow graded GaAsSb layers (on GaAs) to serve as a high quality substrate for LPE growth of subsequent cascade solar cells.

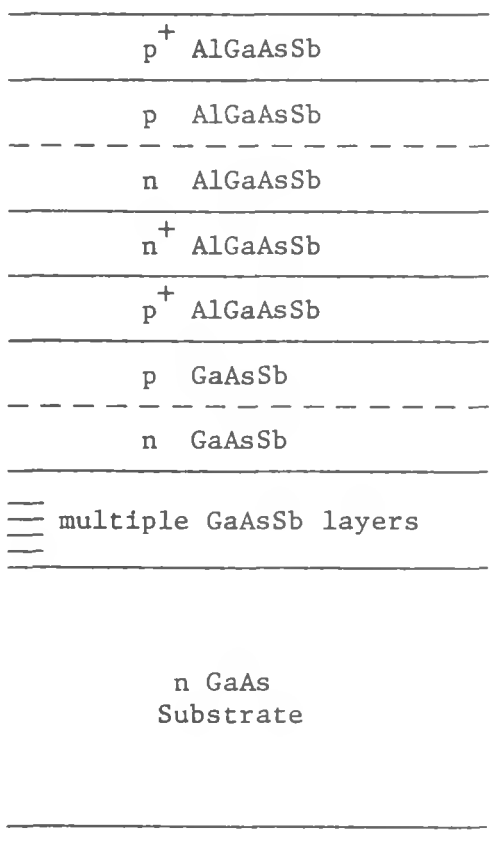

Figure 2.1 GaAlAsSb/GaAsSb Cascade Cell

2.1 Bottom Cell Development

Since it is suspected that the V_{oc} values characterizing the bottom cell may be related to the lattice mismatch with the GaAs substrate, several series of experiments were performed in an effort to address the problem and improve device performance.

The first series of experiments involved growing a number of constant composition layers on top of 4 step-graded layers used for lattice grading and then growing a p-n junction having the same composition as the constant composition layers. The constant composition layers were introduced since there is experimental evidence that dislocations bend horizontally in LPE layers and that dislocation densities are reduced by as much as a factor of 3 to 10 [4]. The results of these growth runs proved fruitful; V_{oc} increased from ~ 0.3 V with no constant composition layers to ~ 0.5 V with six constant-composition layers. Not only did V_{oc} increase but the FF also improved. These results are illustrated in Figure 2.2 by the I-V curves for samples having 0 and 6 constant composition layers.

Further increases in the number of these layers is obviously limited by the number of bins in the graphite boat. An alternate approach is to shuttle back and forth between two melts of identical composition during the growth sequence, permitting growth of as many such layers as desired prior to junction formation. Junctions were grown on structures which had as many as 54 (see Figure 2.3) of these constant-composition layers, but the results of these experiments were not particularly encouraging. The most positive conclusion was that surface morphologies improved and were consistently good for these samples. A record high 1 sun V_{oc} of 0.58 V was measured on one sample (5 step-graded layers, 15 constant composition layers) but this value was only marginally better than a

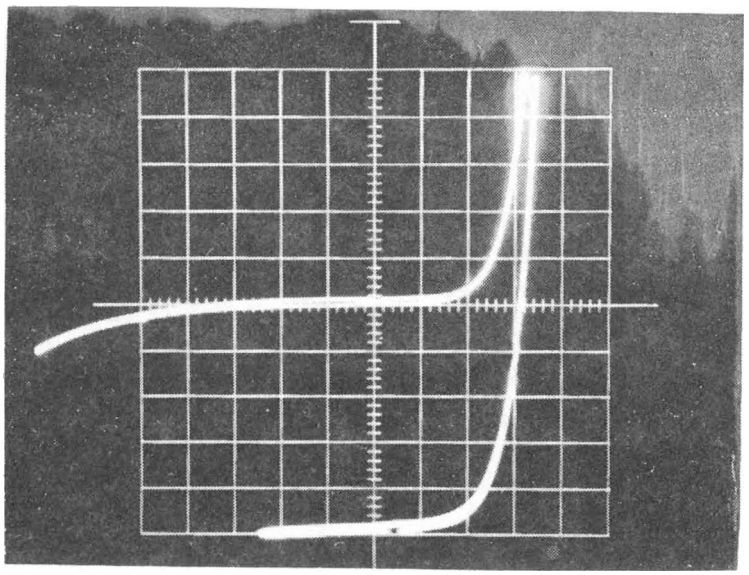

a. 0 constant-composition layers

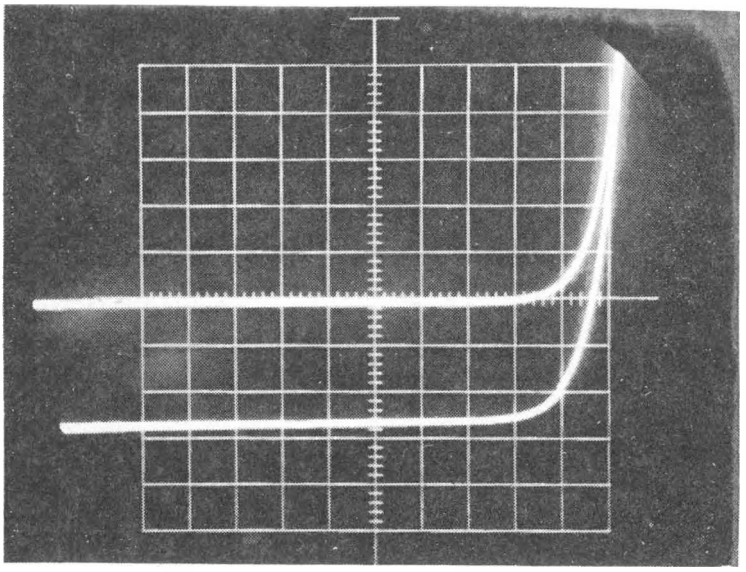

b. 6 constant-composition layers

Vert: 0.1 mA/div

Hor: 0.1 V/div

Figure 2.2 Demonstration of the Effect of Increasing the Number of Constant-Composition Layers Between a GaAsSb Junction and Step-Graded Layers. (Illumination ≈ 11 suns, AM0.)

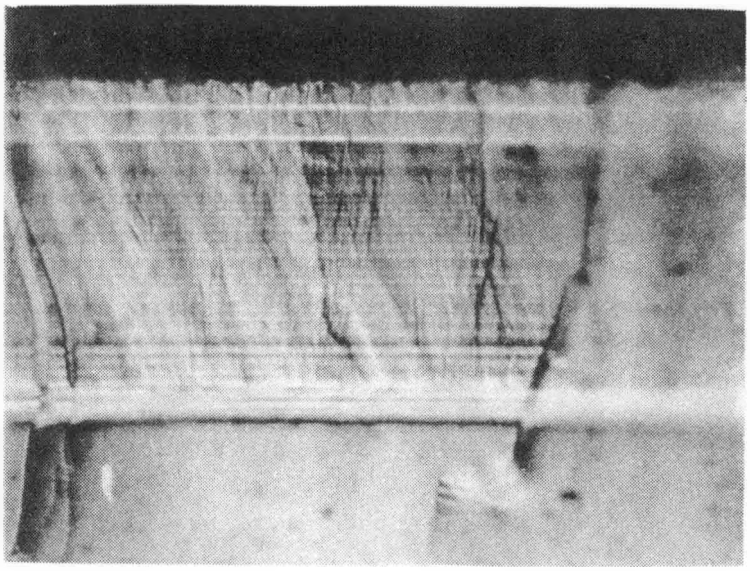

Figure 2.3 GaAsSb p-n Junction (top two layers) Grown on 48 Constant-Composition and 6 Step-Graded Layers.

previous best high of 0.55 V, and the range of measured V_{oc} values (0.45 to 0.55 V) was indistinguishable from the range of values characteristic of samples having only a few constant composition layers. Figure 2.4 shows the I-V characteristic of the best GaAsSb bottom cell. This cell is characterized by a J_{sc} of ~ 8 mA/cm^2 and a diode factor of 1.67; these values are also similar to those of cells with fewer layers. The quantum efficiency shown in Figure 2.5 peaks at ~ 35% and is representative of the better GaAsSb junction.

In considering why there was no further improvement in V_{oc} as the number of constant-composition layers continued to increase, the role of dislocations was further examined. In spite of the excellent surface morphologies, two disconcerting facts were noted about the many-layered

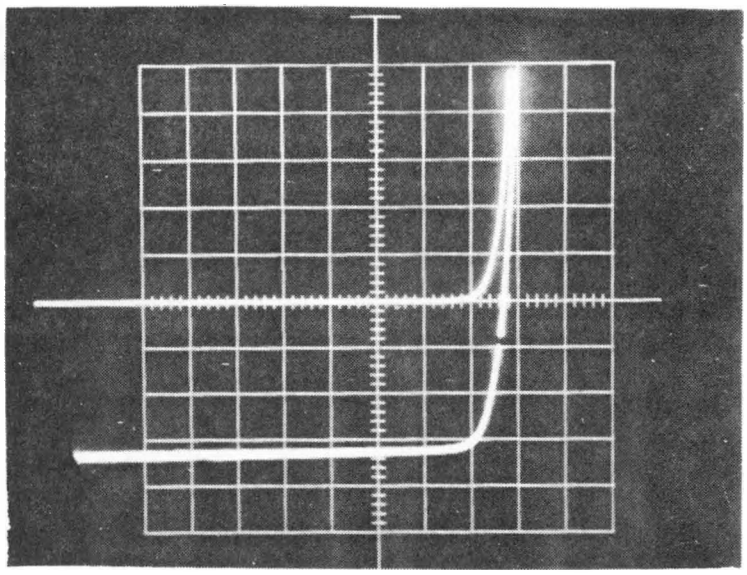

Vert: 0.02 mA/div

Hor: 0.2 V/div

Figure 2.4 I-V Characteristic of GaAsSb p-n Junction Grown on 16 Constant-Composition and 6 Step-Graded Layers. ($V_{oc} \simeq 0.58$ V, $J_{sc} \simeq 8.1$ mA/cm^2)

samples: (1) the photoluminescence (PL) intensity did not increase for these samples, and (2) the etch pit densities (EPD) were still high. Figure 2.6 shows a GaAsSb surface after a 1 minute etch in a cooled solution of HF:CH_3COOH:H_2O_2:H_2O (1:4:2:2) [5]; this solution is reported to produce well formed pits on (111)A and (100) surfaces of antimonide alloys [6]. The EPD is greater than 10^8 cm^{-2} (too high to count accurately), and with EPD's of this magnitude poor device performance is to be expected. The magnitude of the EPD count was disappointing because the surface morphology of this particular sample (#TC115) was one of the best, and there was no apparent EPD difference between this sample and samples grown without the constant-composition layers. Because there is some variation of the EPD from sample to sample and even across the

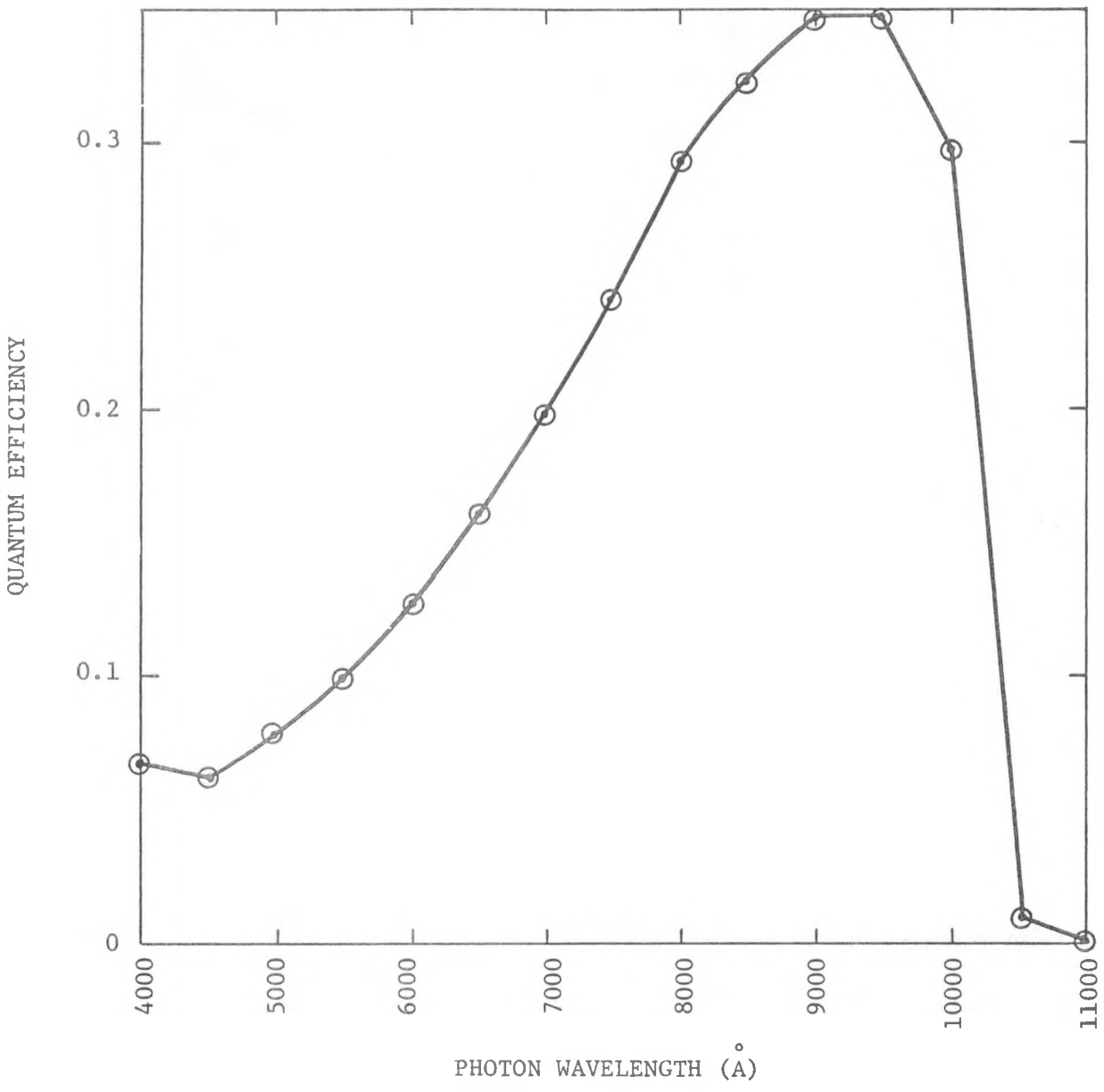

Figure 2.5 Quantum Efficiency of GaAsSb p-n Junction Grown on 14 Constant-Composition and 6 Step-Graded Layers.

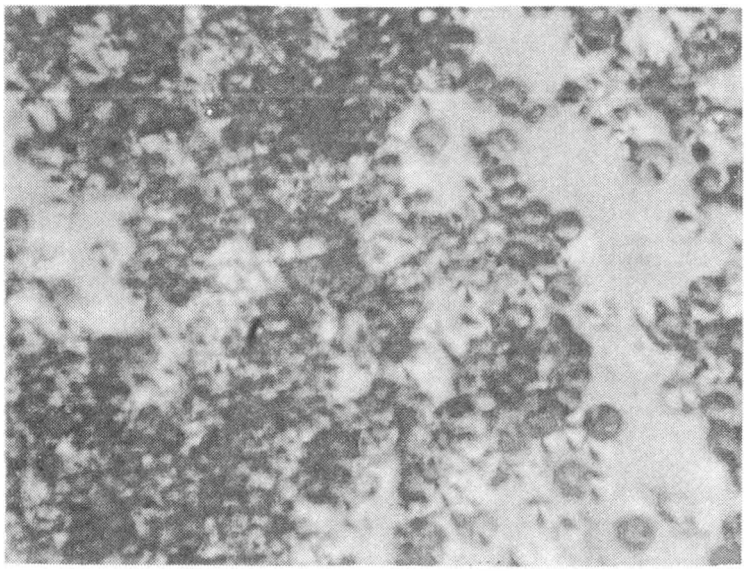

Figure 2.6 Indication of the Etch Pit Density of a Surface of a GaAsSb p-n Junction Grown on 24 Constant-Composition Layers and 6 Step-Graded Layers. (EPD > 10^8 cm^{-2}, 1450×)

surface of a single sample, inconsistent device performance may be the result.

To summarize these experiments, the surface morphologies improved as the number of constant composition layers was increased, but the device performance was essentially identical to GaAsSb cells grown on step-graded layers with only a few constant composition layers. The EPD data supports the work of Moon, et al, who measured EPD counts between 10^6 and 10^8 for single layers of GaAsSb and AlGaAsSb grown directly on (111)A GaAs substrates and layers grown with continuous grading [6]. It is noteworthy that all of this work was done on (111)A GaAs substrates.

Another sequence of experiments involved growth at low temperature (~ 700°C). The lower growth temperatures help reduce the tendency of

the Group V elements (which have higher vapor pressures) to form vacancies and other point defects. These point defects are also potential sources of poor device performance. These experiments, however, were not successful; no single phase crystals were grown at the lower temperatures. These results are in agreement with the work of Lendvay, et al, who reported poor epitaxial growth for GaAsSb and AlGaAsSb below temperatures of ~ 750°C [7]. No further low temperature experiments are planned at present.

In conclusion then, some improvement in device performance has been realized by the addition of several (up to ~ 6) constant-composition layers over the step-graded layers. However, further increases in the number of constant composition layers and LPE growths at lower temperatures did not result in further performance improvements. Dislocations as measured by EPD counts are still too high (> 10^7 or 10^8 cm^{-2}) and are suspected of keeping V_{oc}'s pinned in the vicinity of 0.5 V. Further efforts to improve junction performance by grading techniques will involve OM-CVD experiments.

2.2 Top Cell Development

Low open circuit voltage is also common to AlGaAsSb junctions, and it is anticipated that solving the problem in the ternary bottom cell will very likely lead to improved quaternary junctions. Also, since GaAsSb is easier to grow than AlGaAsSb, this problem is being addressed in the ternary first. In addition to the V_{oc} problem, AlGaAsSb layers have also been characterized by high dislocation densities, as shown in Figure 2.7; this photomicrograph was taken of the etched surface of an AlGaAsSb diode grown on 3 step-graded layers. The equilateral triangular pattern, characteristic of the (111) surface, is apparent and the EPD is

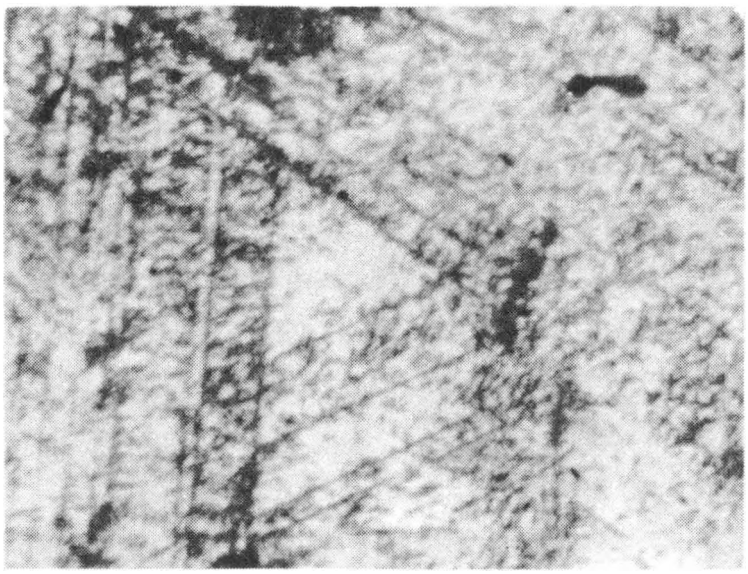

Figure 2.7 Indication of EPD in the Surface of an AlGaAsSb p-n Junction Grown on 3 Step-Graded Layers and a (111)A GaAs Substrate (440×).

too high to count, particularly at this lower magnification (440×). It is believed that this high dislocation density stems in part from the lattice mismatch with the substrate.

2.3 Tunnel Junction Development

Because of tunnel junction interference in the cascade structure, some work with the AlGaAsSb connecting junctions has been undertaken. Tunnel junction improvement has been sought by two means: optimizing the doping levels of the current n- and p-type dopants (Te and Ge, respectively) and seeking new dopants, particularly p-type. Increasing the Ge concentration by 70% in the melt from which the p^+ layer is grown has resulted in 1.7 eV tunnel junctions which have peak current densities

as high as 2.3 A/cm^2. Junctions grown previously with this bandgap had current densities in the mA/cm^2 range; the I-V curve of this junction is shown in Figure 2.8. Further increases in the Ge concentration resulted in samples with unacceptable surface morphologies and poorer performance.

In considering other p-type dopants, the major difficulty is that most potential candidates--Be, Zn, Cd, and Mg--are rapid diffusers and thus it is difficult to grow subsequent layers while retaining the abrupt doping profile and tunneling properties of the tunnel junction. One sample was grown, however, to determine the feasibility of junction formation using a p-type, rapidly-diffusing dopant. Be and Te were used as the p- and n-type dopants, respectively. The forward I-V characteristic of the resulting device is shown in Figure 2.9. In addition to the major peak, some structure in the excess current region is present. The peak current density, J_p, was only 62 mA/cm^2 as compared to the 2.3 A/cm^2 for the diode shown in Figure 2.8 and the differential resistance (dV/dI) near 0 V is 166 Ω as compared to 5 Ω for the Ge-doped diode in Figure 2.8. The performance of the Ge-doped diodes is clearly superior to this Be-doped one, and Ge will be retained as the tunnel junction p-type dopant.

2.4 Cascade Cell Growth Experiments

Most of the effort during the past six months has been directed toward solving the low V_{oc} problem associated with separately grown cells; consequently, there has been relatively little work on complete cascade structures except for some preliminary growth experiments on cascade cells with diffused (rather than abrupt) top and bottom junctions. Although diffused junction cells generally exhibit better junction characteristics, these particular samples had two problems:

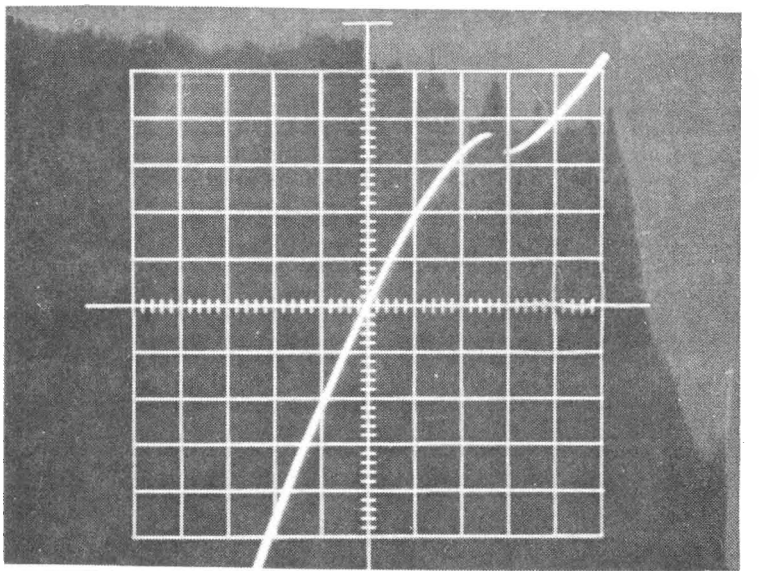

Vert: 20 mA/div

Hor: 0.2 V/div

Figure 2.8 I-V Characteristic of 1.7 eV AlGaAsSb Tunnel Diode (Device area ≈ 3.2×10^{-2} cm^2, J_p = 2.3 A/cm^2)

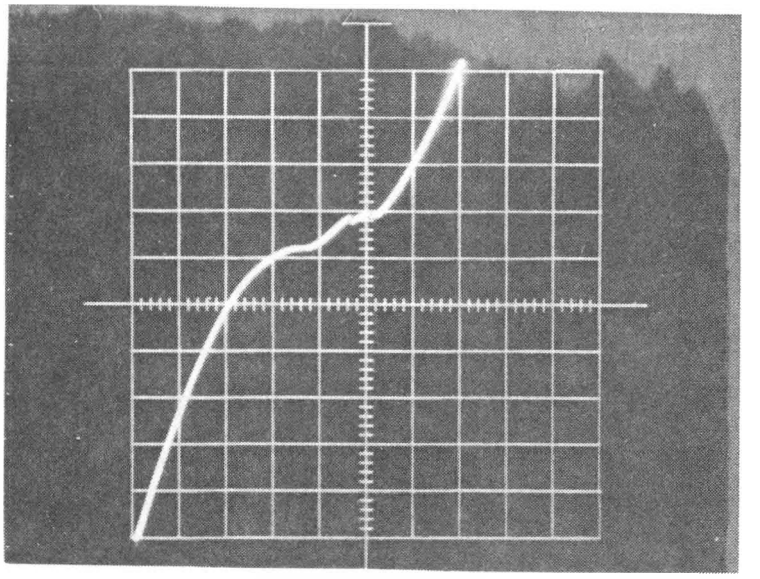

Vert: 0.1 mA/div

Hor: 0.05 V/div

Figure 2.9 Forward I-V Characteristic of AlGaAsSb Tunnel Junction Using Be as the p-type Dopant. (Junction area ≈ 1×10^{-2} cm^2)

shorted top cells, and/or tunnel junction interference. The shorted top cells resulted from poor layer quality caused by insufficient growth times coupled with the slow growth rate characteristic of the AlGaAsSb material; top layer nonuniformity appeared to be further complicated by poor surface morphology of the underlying tunnel junction layers.

Improvements in bottom cell/tunnel junction surface morphologies (as previously discussed) and modification of top layer growth conditions should alleviate this problem in future experiments. (Previous experiments involving cascade cell growth using Ge-doped (abrupt) junctions have been duplicated but these devices are characterized by V_{oc} values on the order of 1 volt as indicated in Figure 2.10).

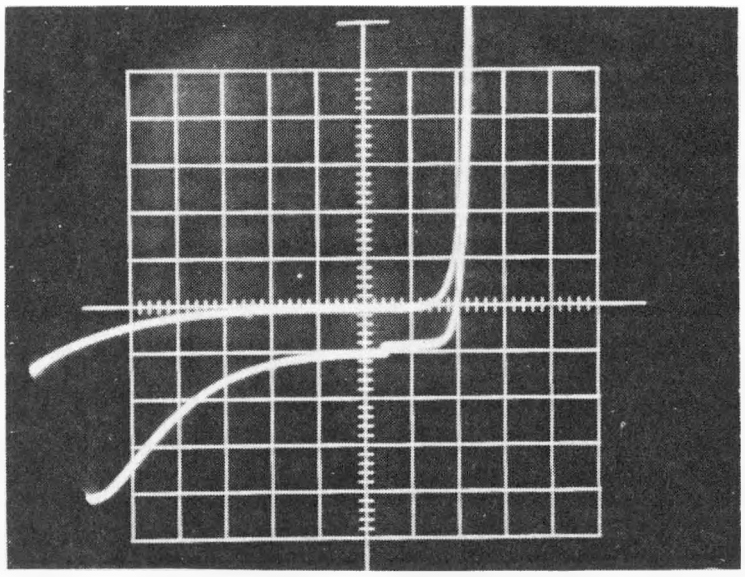

Vert: 0.05 mA/div

Hor: 0.5 V/div

Figure 2.10 I-V Curve of Cascade Structure Grown with Ge-doped (abrupt) Junction. (Illumination ≈ 10 suns, AM0)

2.5 OM-CVD Growth of GaAsSb

Efforts to improve bottom and top cell performance have been directed primarily towards reducing the number of dislocations resulting from the ~ 0.8% lattice mismatch between the GaAs substrate and the GaAsSb bottom cell. Several different schemes using LPE have been tried, but the dislocation density (as indicated by EPD counts) is still very high. Even when using an effective continuous grading technique, Moon, et al, report EPD's > 1×10^6 cm^{-2} for LPE growth on (111)A GaAs substrates [6]. The OM-CVD growth technique offers some advantages for compositional grading as indicated below:

1. Very thin layers can be grown reproducibly,
2. Surface morphologies tend to be superior to those of LPE, and
3. OM-CVD, unlike LPE, is not an equilibrium process and compositions even in the miscibility-gap range of the Ga-As-Sb system can be and have been grown.

The OM-CVD growth effort has had several major goals. First, it is necessary to grow the compositions of interest for grading between the substrate and bottom cell. This particular goal has presented few problems since the bottom cell is $GaAs_{1-x}Sb_x$ (x = .13), a composition well outside the miscibility gap. In fact, compositions as high as x = 0.70 have been grown. Therefore, ternary composition does not appear to be a problem.

Almost as important as the composition is the surface morphology since other layers will be grown on the graded ones. The OM-CVD growths have generally had excellent morphologies and a typical example is shown in Figure 2.11. The surfaces are mirrorlike and are quite sensitive to substrate preparation--the cleaner and more perfect substrates yield

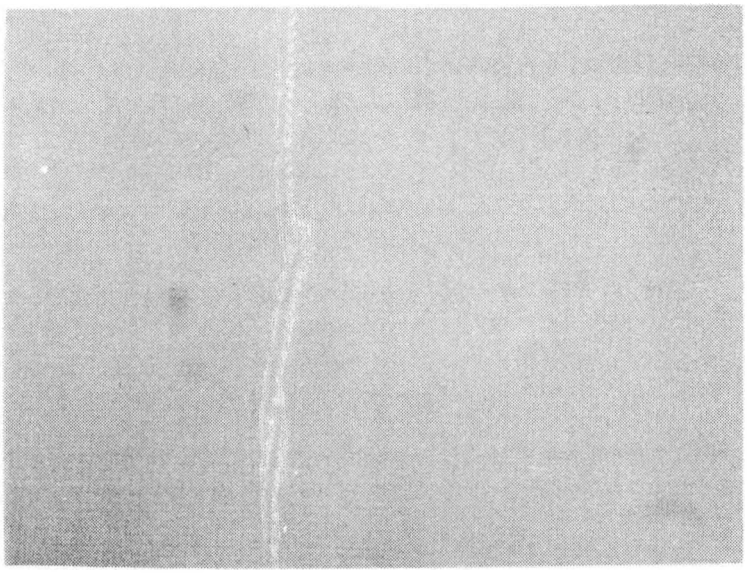

Figure 2.11 Surface Morphology of $GaAs_{0.87}Sb_{0.13}$ Layer Grown on (100) GaAs (2° toward (110)) (150×). Cross-hatching characteristic of this substrate orientation. 6 step-graded layers are included in the structure.

better epitaxial layers. The cross-hatched pattern is characteristic of the (100)-oriented substrate (2° toward (110)), and these surfaces appear identical to those reported by Cooper, et al, in their investigations of OM-CVD grown GaAsSb [8]. The surface morphologies have remained good for $x \simeq 0.30$ but are degraded above this value as the mismatch becomes quite severe (> 2%).

In addition to good surface morphology, the intensity of the PL response has been strong for the OM-CVD grown material and, in fact, has been as strong as that of LPE-grown material of the same composition in most cases. The full-width-at-half-maximum (FWHM) numbers have been quite good--in the range of 40 to 70 meV--and a plot of FWHM vs the room temperature bandgap (determined by PL) is shown in Figure 2.12. This

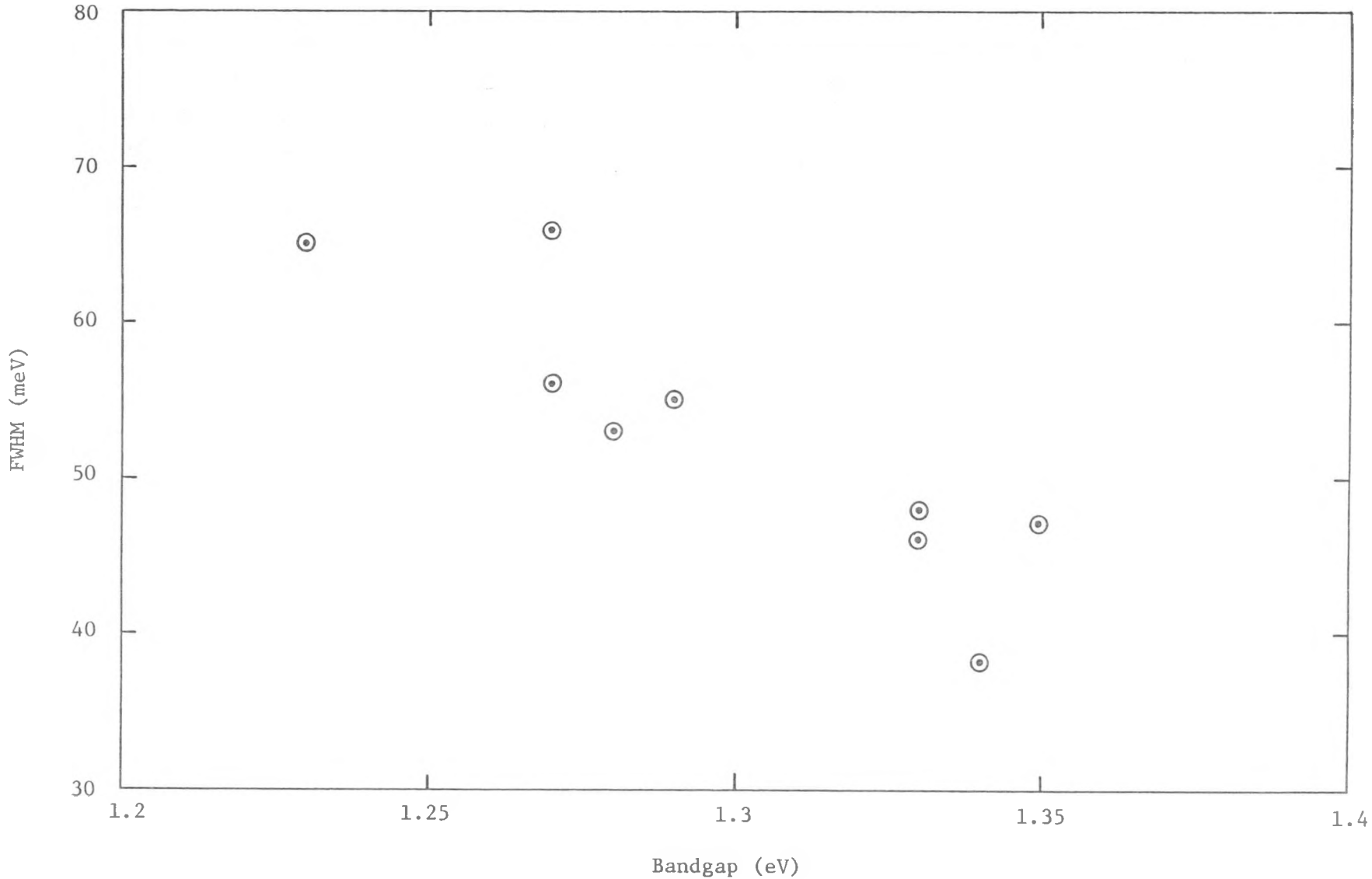

Figure 2.12 Full-width-at-half-maximum vs Bandgap of OMCVD-grown GaAsSb.

plot shows an increase in FWHM as the Sb incorporated into the grown layers increases, i.e., as the bandgap decreases. These FWHM values are, nonetheless, lower than those of LPE-grown material which have typically ranged from 65 to 110 meV, almost a factor of 2 greater than that of the OM-CVD samples. This provides an indication of the high crystalline perfection of the OM-CVD grown samples.

Hall measurements performed on unintentionally doped GaAsSb layers grown on Cr-doped substrates indicated that the material was p-type with carrier concentrations in the mid-10^{16} cm^{-3} range. This was somewhat surprising and may be the result of impurities in the trimethylantimony bubbler and the relatively high Group III/Group V ratio which is used in these growths. Further work on this aspect of the OM-CVD growths will continue.

After it was established that the compositions of interest could be easily grown, multi-layered growths were then initiated. Figure 2.13 illustrates a cleaved, stained cross-section of a sample consisting of a GaAs buffer layer, seven step-graded layers, and three constant composition GaAsSb layers (15.6% GaSb). The layers are very uniform and reproducible. The total structure is about 7.9 μm thick, the growth rate being ~ 0.12 μm/min with the conditions being used.

Growth on (111) GaAs was then initiated because this has been the substrate most frequently used for the LPE growth, and one objective of the OM-CVD experiments is to effect the necessary lattice matching by OM-CVD, and then grow the active layers of the cascade structure by LPE to take advantage of the superior electrical properties that are generally associated with LPE layers. OM-CVD growth on the (111)A face has been accomplished, but the surface morphology is not as good as that of the

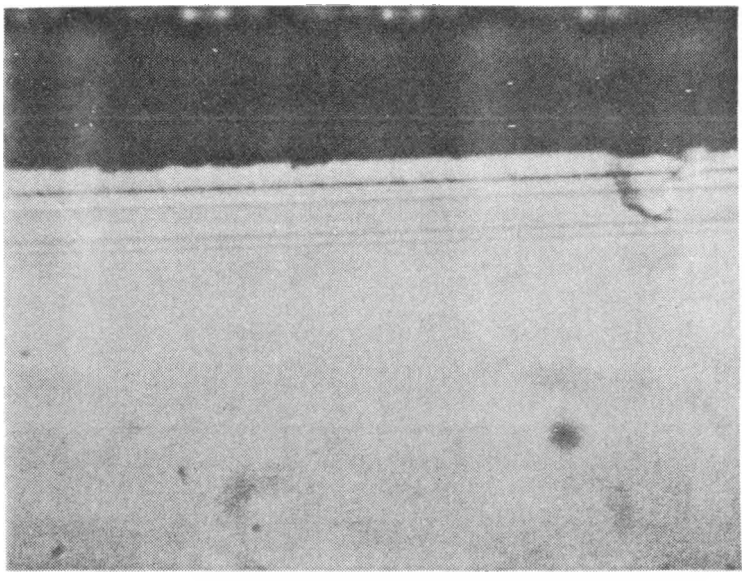

Figure 2.13 Cleaved, Stained Cross-section of OMCVD-grown, Multilayered Structure (1450×).

(100) face. One of the best (111) surfaces is shown in Figure 2.14, which compares (111) and (100) surfaces that were grown at the same time. An interesting note about the composition of these layers is that there is a 2 to 3% greater increase in Sb incorporation on the (111)A surface than on the (100) one, and this trend has been seen consistently when (100) and (111) samples are grown side by side. The (111)B surface has yielded only polycrystalline material to date.

Perhaps the most meaningful result of these experiments has come from a comparison of EPD's for the two orientations. Photomicrographs (1450×) of (100) and (111)A surfaces after etching in the $H_2O:H_2O_2;CH_3COOH:HF$ solution for 25 sec and 90 sec, respectively, are shown in Figure 2.15. Here, the EPD count is far greater for the (111)

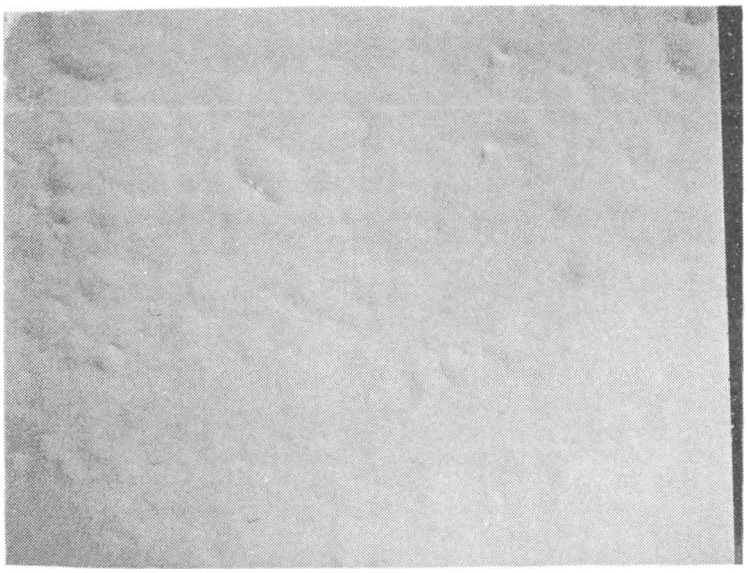

a. (111)A GaAs substrate (300×)

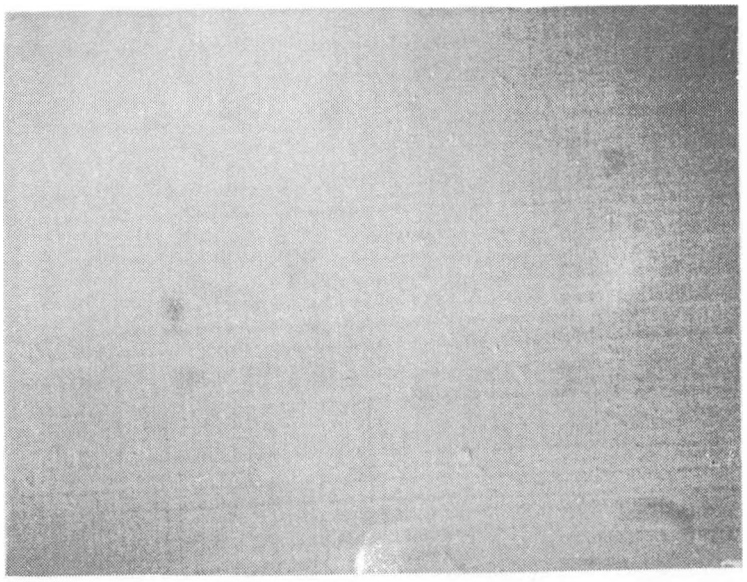

b. (100) GaAs substrate (300×)

Figure 2.14 Photomicrographs of GaAsSb Layers Grown Simultaneously on (100)- and (111)-GaAs Substrates.

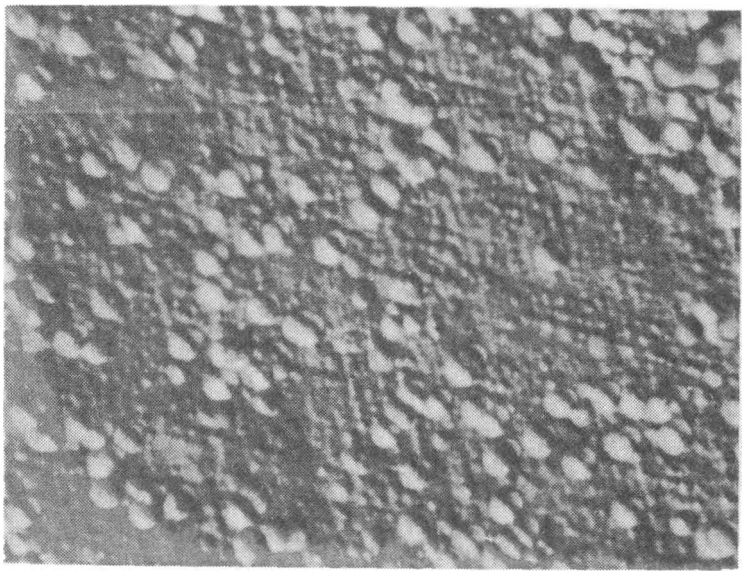

a. (111) GaAsSb surface (1450×): 25 sec etch

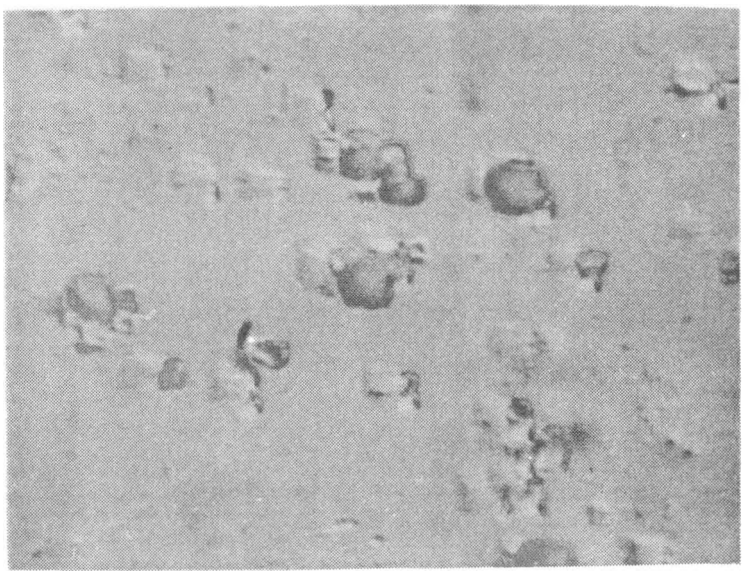

b. (100) GaAsSb surface (1450): 90 sec etch

Figure 2.15 Etch Pits for (111)- and (100)-GaAsSb Surfaces.

surface, and it looks very much like the EPD pattern for the best LPE layers. The pit count is far lower on the (100) surface, and there were significant areas of this (100) surface which had far fewer pits than is shown in the photomicrograph.

This finding led to a very careful examination of the pit densities of (100) surfaces. These densities have ranged from 6×10^6 cm^{-2} to 1×10^6 cm^{-2}. A very typical pattern is shown in Figure 2.16 where the EPD is ~ 2×10^6 cm^{-2}; here, as with the first comparison, there are areas where the pitting is more dense and considerable areas where the pitting is less dense. This variation in pit density very easily explains the difference in junction performance from mesa to mesa in the same substrate and from substrate to substrate. This represents a dislocation reduction of at least two orders of magnitude over the (111) LPE and the (111) OM-CVD samples, and it is hoped that better device performance will result from this significant reduction in dislocation density.

As a final note of comparison, a (111) GaAsSb surface is shown in Figure 2.17 before and after a 40 sec EPD etch. Also shown in this figure are enlarged areas after 20 sec and 40 sec of etching. A comparison of Figure 2.17 with Figure 2.16 emphasizes the reduction in EPD characteristic o material grown on (100)-oriented substrates.

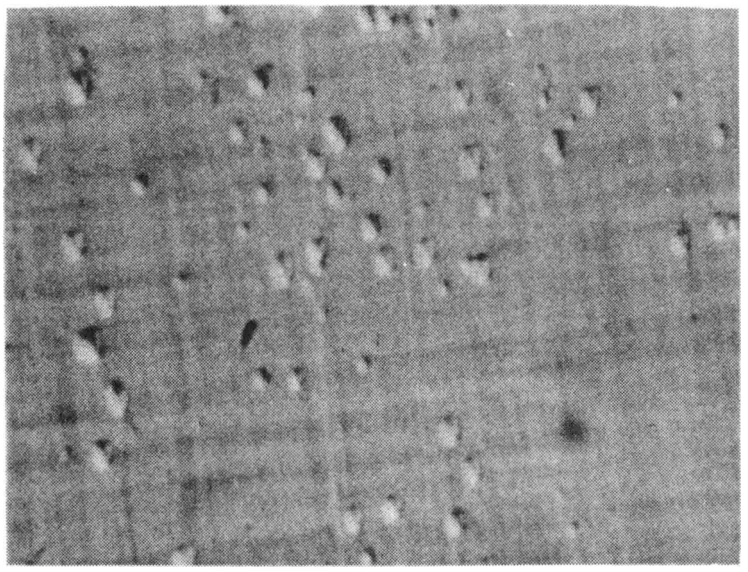

Figure 2.16 Etch Pits of Typical (100) GaAsSb Layer (EPD $\simeq 2 \times 10^6$ cm^{-2})

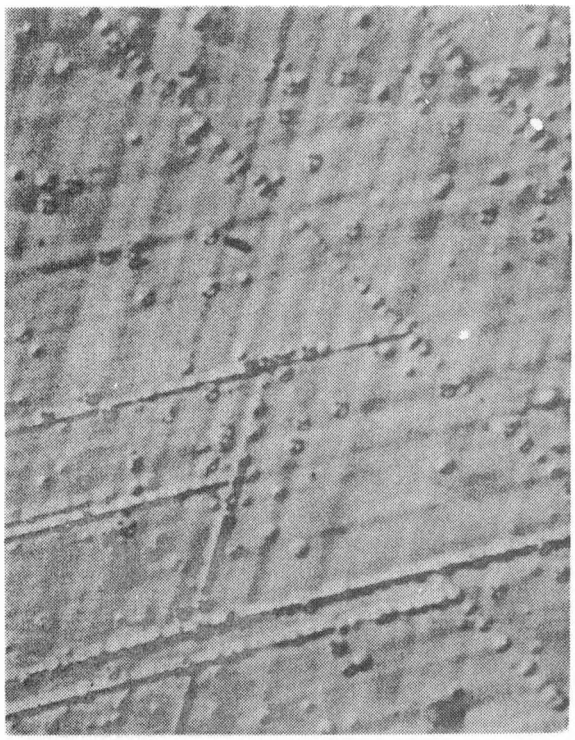

a. Etched 20 sec (1450×)

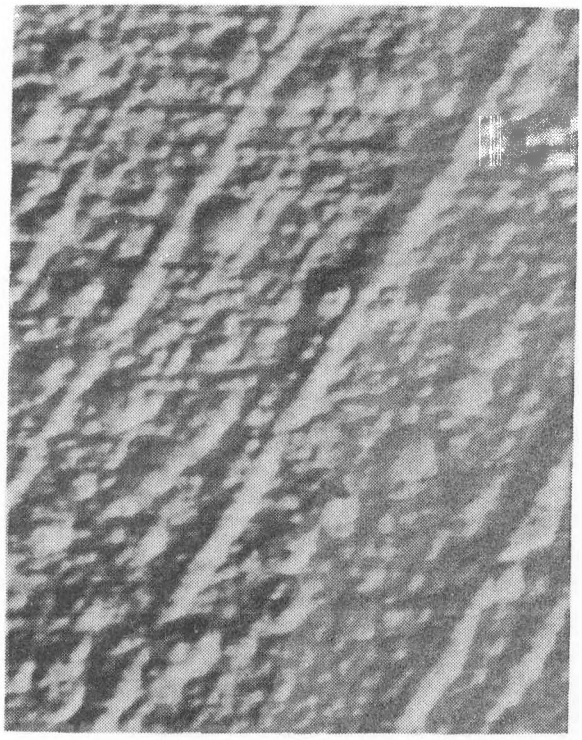

b. Etched 40 sec (1450×)

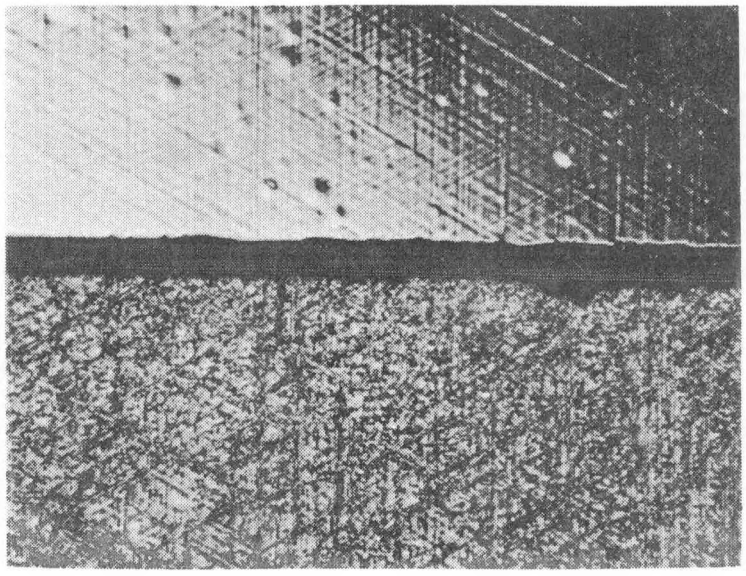

c. (111) GaAsSb layer before (top) and after 40 sec etch (710×)

Figure 2.17 Effect of Etching on (111) GaAsSb Layers

2.6 Conclusions

The following is a summary of the results of the GaAsSb/GaAlAsSb work during this report period:

1. Several grading schemes using LPE have been tried which resulted in surface morphology improvement; the use of several step-graded layers plus a few constant composition layers appears to improve junction V_{oc}.
2. Tunnel junction performance has been improved by increasing the p-type dopant concentration in the melt. Dopants which diffuse rapidly do not appear to give performance nearly as good as Ge-doped layers.
3. Initial growth experiments on complete cascade structures with diffused junctions resulted in structures with shorted top cells. Growth conditions will be modified to improve top layer quality.
4. Good quality OM-CVD GaAsSb layers have been grown on (100) GaAs. The PL intensity is comparable to the best LPE material, surface morphologies are excellent, and layers are very uniform and are grown reproducibly. The necessary compositions have been grown on both (100) and (111)A substrates for lattice matching. The EPD's of (111) surfaces are about 2 orders of magnitude higher than the (100) surface for samples which were grown at the same time, and this is probably the most significant result of this report period.

3.0 AlGaAs/GaAs Cell Development

Although the 1.92/1.43 eV top cell/bottom cell bandgap values for this cascade structure do not correspond exactly to the optimum values of 1.8/1.2 eV for a two-junction concentrator cell, computer modeling studies of the AlGaAs/GaAs cell (see Section 4.0) show that it can meet or exceed the efficiency goals of the present contract.

The structure under development is depicted in Figure 3.1 and consists of Be diffused top and bottom cell junctions of AlGaAs and GaAs, respectively, which are connected together by an AlGaAs tunnel junction. The AlGaAs window layer used with the bottom cell serves to provide better control of Be diffusion during junction formation [2].

Efficiencies of the best experimental cells have remained around 15-16% (1 sun, AM1.5, without AR coatings). When equipped with a two-layer AR coating, these values should increase to the 20 to 21% range; this compares with a projected efficiency of approximately 27% for the AlGaAs cell.

The major factors limiting performance of experimental cells appear to be directly or indirectly related to the tunnel junction. Specifically, these involve 1) poor tunnel junction performance due either to an optically active junction or to poor ohmic contact and 2) poor top cell performance resulting from dislocations introduced into upper LPE layers by defects in the highly doped tunnel junction layers. Consequently, efforts during the past six months have focused on improving tunnel junction and top cell performance.

The following observations have resulted from recent work:

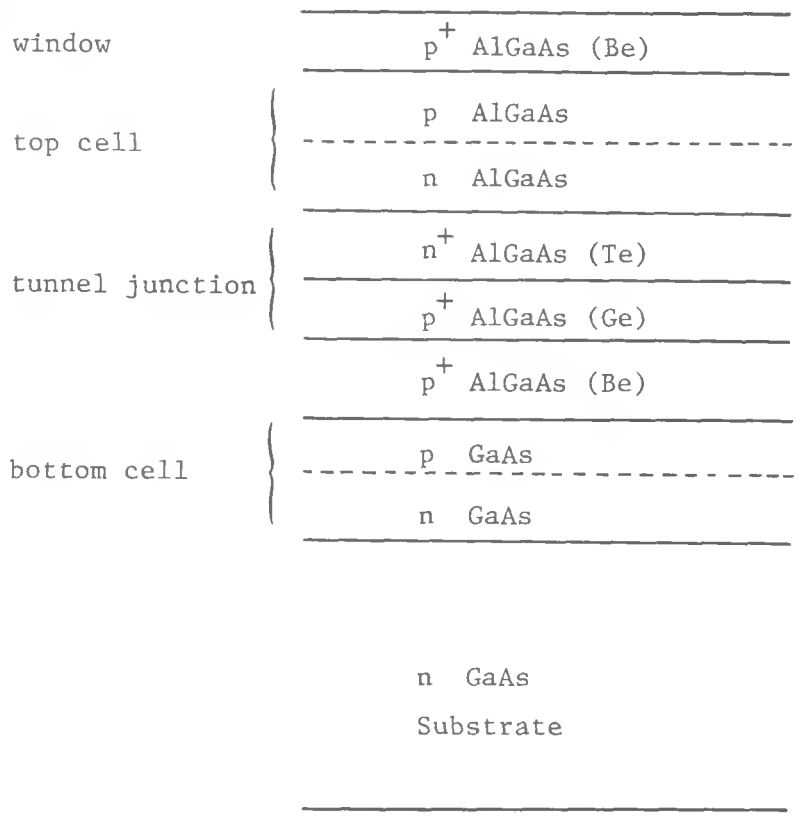

Figure 3.1 GaAlAs/GaAs Cascade Cell

- The atomic fraction of Be in the $Al_{0.9}Ga_{0.1}As$ window layer is fairly critical. A very high atomic percent (greater than 0.1%) in the AlGaAs melt results in excessive Be diffusion and produces a top cell diffused junction depth greater than several microns. For Be less than 0.01 atomic percent, the carrier concentration in the window layer is usually in the high 10^{17} cm^{-3} range, and no noticable diffusion of Be into the n-$Al_{0.3}Ga_{0.7}As$ layer is observed. These results indicate that the diffusion of Be depends heavily on its concentration.
- Best results (in terms of diffused AlGaAs junctions) have been obtained with Be in the range of 0.02 to 0.06 atomic percent. These values include the unavoidable losses of Be due to the presence of water vapor and oxygen in H_2 flowing in the LPE reactor.
- It has been noticed consistently that any minor leaks in the system result in V_{oc} values of $\simeq$ 0.5 V for material having a bandgap of 1.9 eV.
- SEM and EBIC scans on cleaved junctions showed that low V_{oc} values are associated with a p-$Al_{0.9}Ga_{0.1}As$/n-$Al_{0.3}Ga_{0.7}As$ heterojunction (rather than a junction diffused beneath the interface) where a high density of defect are present. For a sample with $V_{oc} \geq 1$ V, a diffused junction with a junction depth in the range from 1 to 2 μm was observed. The best V_{oc} for a $Al_{0.3}Ga_{0.7}As$ junction was 1.32 V.

The open circuit voltage of both top and bottom cells was improved by doping the n-side of the junctions with Sn to the mid $10^{17}/cm^3$ range. This has resulted in a cascade cell V_{oc} of 2.21 V at one sun, without the effect of the nonlinear part of the tunnel junction. The corresponding FF for this 2.21 V_{oc} cell is about 0.78; this is the best (FF) (V_{oc}) product obtained so far. The short circuit current for this run was only about 10 mA/cm^2. The V-I characteristic for this sample is shown in Figure 3.2.

Another sample recently exhibited a current density of 13.6 mA/cm^2 (AM0, 1 sun, no AR coat), which is a record high for the AlGaAs/GaAs cascade cell during this project. Unfortunately, this sample was characterized by a V_{oc} of only 2.05 V and the fill factor was relatively low ($\simeq$ 0.7). Figure 3.3 illustrates the spectral response measured for this cell.

A multiple well LPE boat capable of handling 2 × 2 cm substrates has been designed and fabricated and LPE growth runs have been initiated on the larger substrates. (Runs are continuing on 1 × 1 cm substrates.) Initially, a GaAlAs top cell (E_g = 1.8 to 1.9 eV) was grown to check out the growth system. Be was diffused from an $Al_{0.9}Ga_{0.1}As$ window to form the junction. Surface morphology across the 2 × 2 cm substrate was very good. The substrate was subsequently sliced into four 1 cm^2 samples. Ohmic contact to mesa structures across one sample showed open circuit voltages in the range of 1.25 to 1.31 V for almost all the mesas. Short circuit currents in the range of 13 to 15 mA/cm^2 were measured on all the mesas. This 2 × 2 cm substrate run has been repeated and essentially the same results were obtained. More recently, complete cascade cells

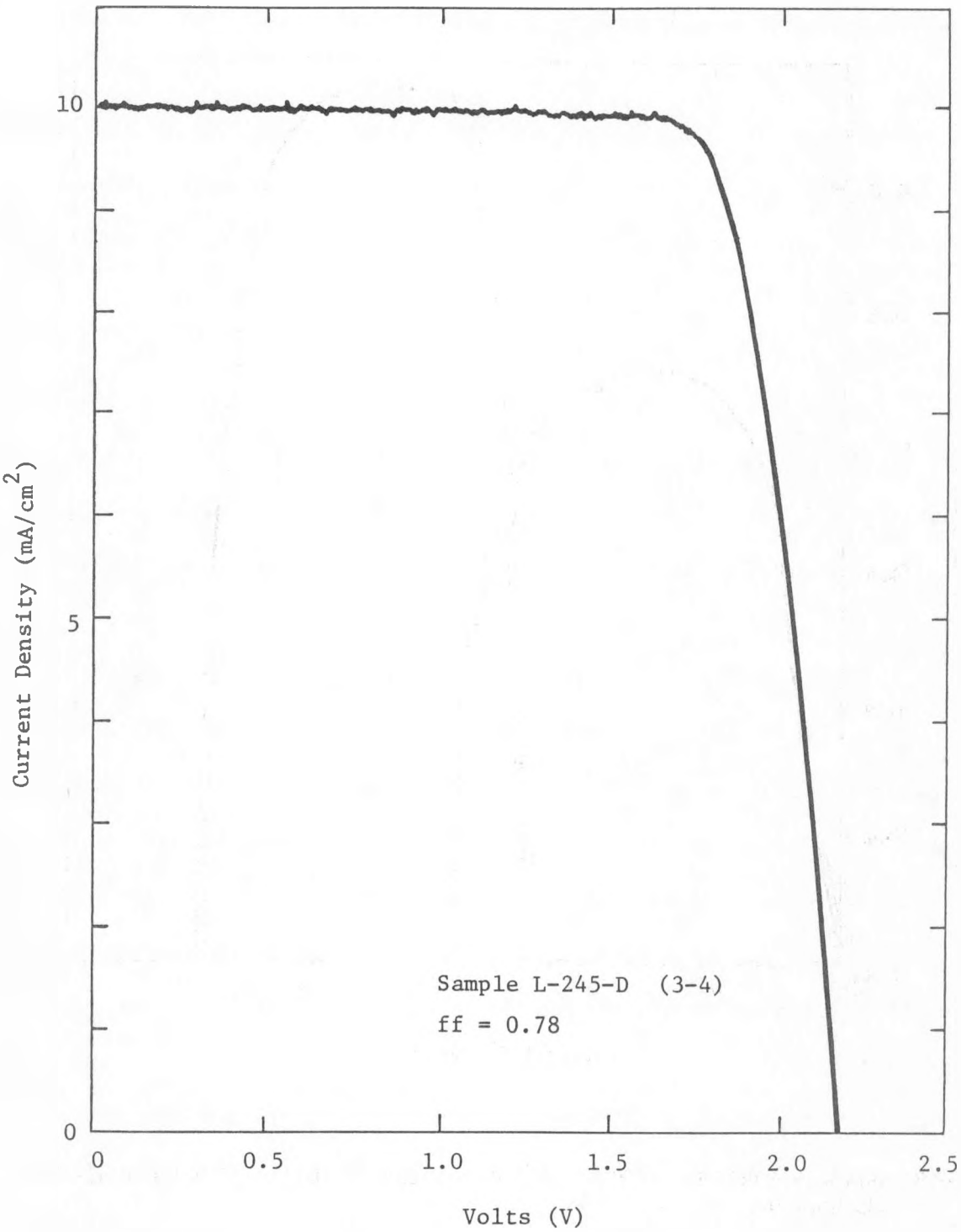

Figure 3.2 V-I Characteristic for AlGaAs/GaAs Cascade Structure

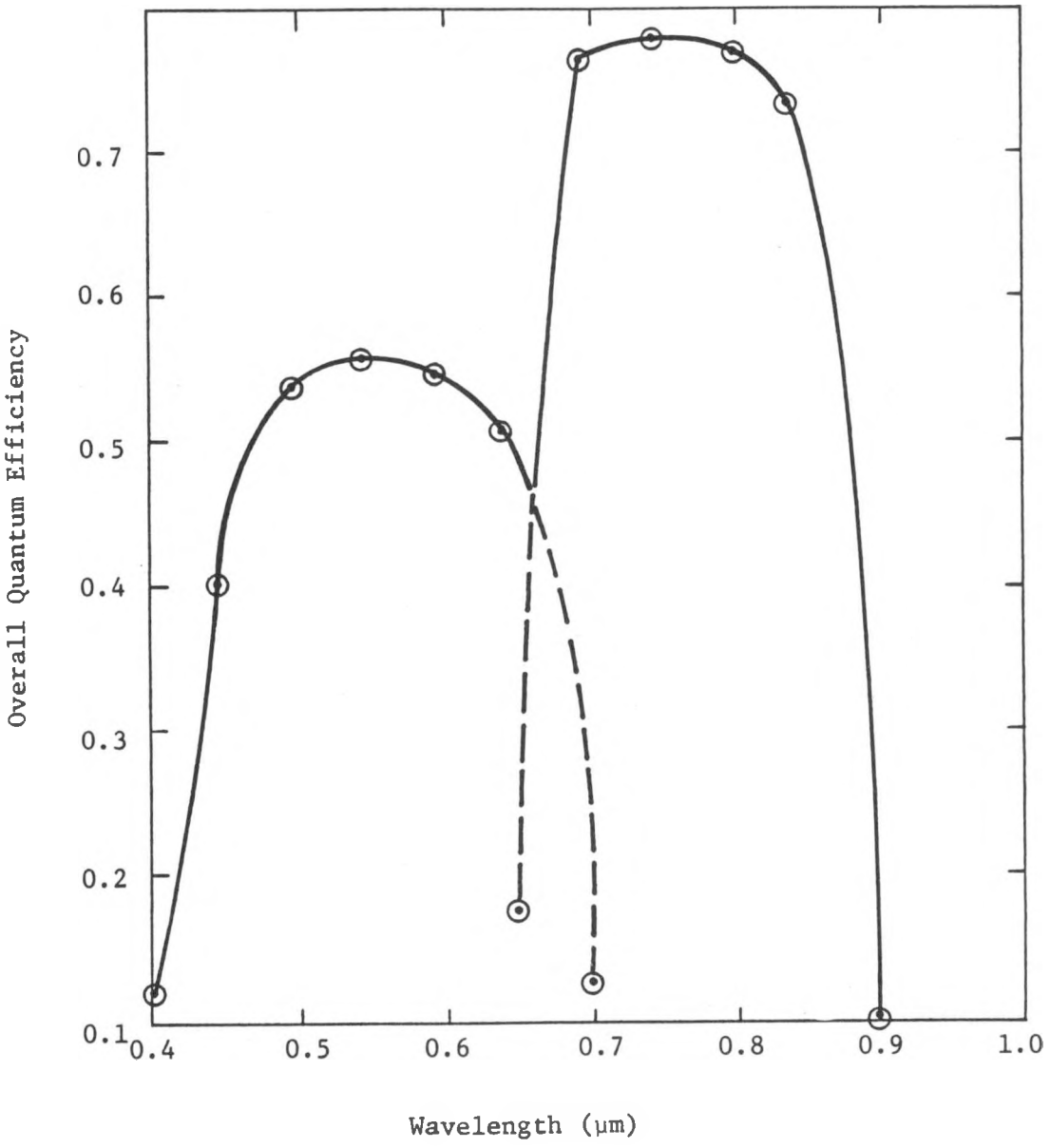

Figure 3.3 Quantum Efficiency Measured on Cascade Solar Cell Sample R-239-C (3-4) Without AR Coating

have been fabricated on the 2 × 2 cm substrates. These runs will be evaluated after each wafer is processed into 12 × 12 mesa array of small area cells.

4.0 Computer Modeling of AlGaAs/GaAs Cell for High Solar Concentration

This section describes the results of a computer modeling study of the AlGaAs/GaAs (1.9 eV/1.44 eV) cascade cell. Performance data are calculated for this cell operating over a temperature range of 300 K to 600 K at various solar concentrations ranging from 1 to 500 suns (AM1.5).

4.1 Analytical Technique

The technique employed in this analysis has been previously described in some detail [8-11]. The basic approach involves closed form solution of the transport equations with the general solution obtained for the integral form of the continuity equation. Minority carrier concentrations are obtained from the general solutions subject to the appropriate boundary conditions for each distinct region. The procedure then gives combined as well as individual V-I curves from which other performance parameters can be derived. The analysis was implemented on an IBM 370-165 computer.

The following assumptions and/or approximations were used in this analysis:

1. the thermal diffusion contribution to dark current is large compared to space-charge recombination and excess tunnel current components in the top and bottom cells
2. the minority-carrier recombination rate is linearly proportional to excess carrier concentration
3. recombination at heterojunction interfaces are negligible
4. efficiency is not corrected for grid contact shadowing or for power loss from joule heating arising in the structure's series resistance

5. reflectivity at the window surface is assumed to be 5% for all wavelengths

6. the surface recombination velocity is assumed to be 10^6 cms^{-1}

7. a series resistance of 5×10^{-3} ohms-cm^2 is used in the program.

The analysis was conducted on the structure depicted in Figure 4.1 for air mass 1.5, solar concentrations ranging from 1 to 500 suns, and for a temperature range of 300 K to 600 K.

4.2 Results and Discussion

Figure 4.2 shows the calculated cascade cell efficiency (η_c) as a function of temperature for 1 and 500 suns, respectively. Also shown are the individual efficiency contributions from the top and bottom cells. In addition, the normalized efficiency temperature coefficient (γ_e) is given for each of the curves; this coefficient is equal to the normalized slope of the respective curves [8,9]

$$\gamma_e = \frac{1}{\eta(300\ K)} \frac{d\eta}{dT} \quad , \qquad (1)$$

where η is the cascade or component cell efficiency. These results are typical of those obtained for other material combinations operating under air mass exposures ranging from 0 to 5 and in the same temperature range [3,9,10].

An expected observation made from Figure 4.2 is that the cascade and component cell efficiencies increase with increasing solar concentration for a given temperature, as listed in Table 4.1. While the improvement realized in going from 1 to 500 suns is 11% to 12% at 300 K for the cascade and top cell efficiencies, it is 18 to 19% at 400 K. Correspondingly, the improvement is 16% at 300 K for the bottom cell,

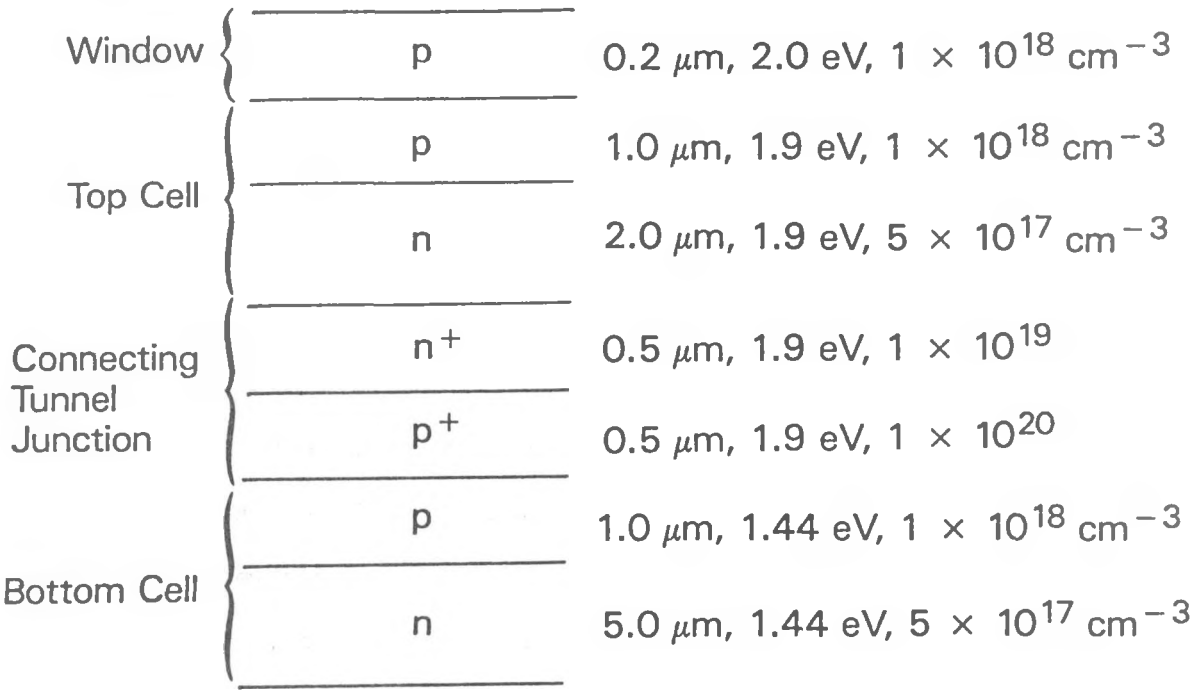

Figure 4.1 Cross section of AlGaAs/GaAs cascade solar cell used in the computer modeling study.

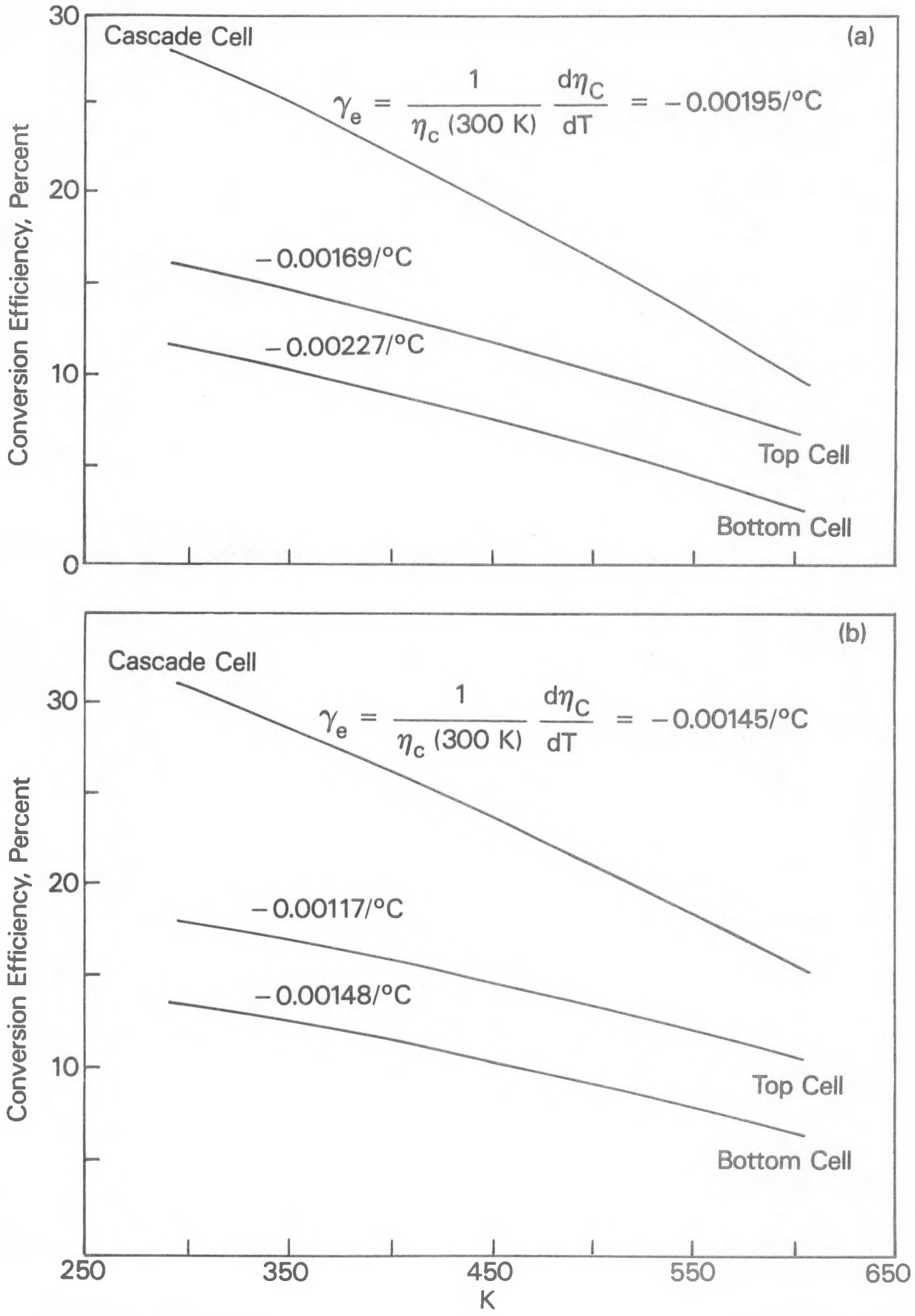

Figure 4.2 Conversion efficiency vs. temperature: a) 1 sun; b) 500 suns.

TABLE 4.1 SUMMARY LISTING OF CONVERSION EFFICIENCIES FOR 1 SUN AND 500 SUNS AND FOR 300 K AND 400 K

Temperature (K)	Solar concentration (suns)	Cascade cell efficiency (%)	Percent increase	Top cell efficiency (%)	Percent increase	Bottom cell efficiency (%)	Percent increase
300	1	27.63	11.1	16.00	11.8	11.60	16.4
	500	30.72		17.90		13.50	
400	1	22.23	18.2	13.30	18.8	8.97	28.0
	500	26.28		15.80		11.50	

TABLE 4.2 SUMMARY LISTING OF PHOTOVOLTAGES FOR 1 SUN AND 500 SUNS AND FOR 300 K AND 400 K

Temperature (K)	Solar concentration (suns)	Cascade cell V_{mpC} (V)	Percent increase	Top cell V_{mpT} (V)	Percent increase	Bottom cell V_{mpB} (V)	Percent increase
300	1	2.36	11.1	1.36	11.7	0.99	16.2
	500	2.62		1.52		1.15	
400	1	1.88	18.6	1.12	19.6	0.76	28.9
	500	2.23		1.34		0.98	

and 28% at 400 K. The major factor leading to higher efficiency is the corresponding increase in photovoltage as the solar concentration is increased. This is shown in Table 4.2, where the photovoltage increments correspond very nearly to the efficiency increment values listed in Table 4.1.

A second observation from Figure 4.2 is that the normalized temperature coefficient value represented for the cascade cell lies between the values of the top and bottom cells. Similar results have been presented and discussed for the two-junction AlGaAs-GaInAs cascade cell [3,9]. Although the efficiency temperature coefficient has been discussed in the literature, it has not been studied extensively and its importance is not universally recognized. For applications in which the solar concentration and/or the ambient temperature are high, this parameter takes on an additional importance. Table 4.3 compares the normalized efficiency temperature coefficients taken from Figure 4.2 with values taken from the literature for the two-junction AlGaAs-GaInAs cascade cell and for single junction AlGaAs/GaAs and Si cells.

TABLE 4.3 **PARTIAL LISTING OF THE NORMALIZED EFFICIENCY TEMPERATURE COEFFICIENCY FOR SINGLE- AND TWO-JUNCTION CASCADE SOLAR CELLS**

Material	Number of active junctions	Solar concentration, c (suns)	Normalized efficiency temperature coefficient, γ_e $(°C)^{-1}$
AlGaAs-GaAs	2	1-500	-0.00145 to -0.00195
AlGaAs-GaInAs [6,7]	2	1	-0.00220 to -0.00270
AlGaAs/GaAs [12,13]	1	1	-0.0027
Si, p/n [12, 14]	1	1	-0.0047
Si, n/p [12, 14]	1	1	-0.0050

Values for the AlGaAs/GaAs and Si single junction cells were calculated from experimental data [11], while the cascade values are obtained from computer modeling [3,10]. However, the computer modeling program used in this study predicts a value of -0.0025/°C for the single junction AlGaAs/GaAs heteroface cell; this represents a 7% disagreement between experimental and computer modeling. The disagreement between these values may be reduced if the complete set of parameters of the experimental structure were known. Moreover, the present program has shown agreement to within less than 0.5% with the experimentally observed photovoltage temperature coefficient for a two-junction AlGaAs/GaAs cell. Therefore, we have confidence that the computer modeling results obtained for cascade cells are a fair to good representation.

Table 4.3 shows that the single junction AlGaAs/GaAs coefficient is approximately one-half the Si value. Further, the cascade cell values are significantly lower than the single junction AlGaAs/GaAs coefficients for all values of solar concentration listed. Also, the normalized values shown in Figure 4.2(b) for 500 suns are considerably lower than the 1 sun values for both cascade and component cells; this is because the photovoltage temperature change becomes less significant at higher concentrations.

In Figure 4.3, the temperature behavior of the photovoltage at the maximum power point of the V-I curve is shown for the cascade (V_{mpC}), top (V_{mpT}), and bottom (V_{mpB}) cells at 1 and 500 suns. The normalized slopes, representing the normalized photovoltage temperature coefficients (γ_V), are also shown.

It should be noted that the photovoltage temperature behavior in a cascade cell is the major parameter responsible for the behavior of

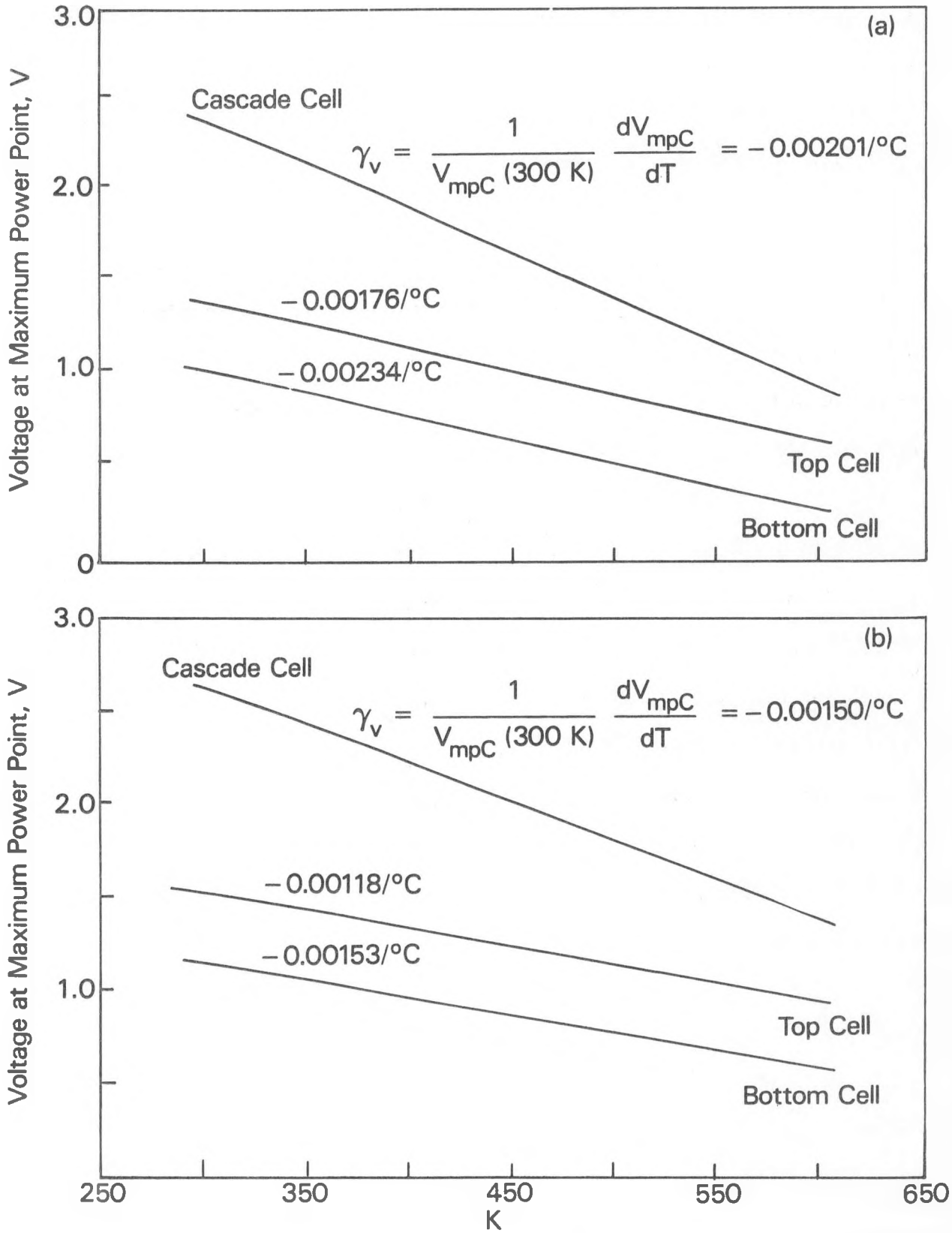

Figure 4.3 Voltage at the maximum power point vs. temperature a) 1 sun; b) 500 suns.

efficiency with temperature. It is also seen that the normalized efficiency and photovoltage temperature coefficients decrease at about the same rates with increasing solar concentration. (A similar result is obtained for single junction solar cells.) However, because of the improved temperature performance characteristics of solar cells operating under high solar concentrations, these applications take on new importance.

The behavior of efficiency and photovoltage with increasing solar concentration (log scale) are shown in Figures 4.4 and 4.5, respectively, for 300 K and 400 K. It is clear that all curves exhibit a monotonic increase with increasing solar concentration.

The behavior of photocurrent and dark current with increasing solar concentration are shown in Figure 4.6. While the short-circuit current (J_{scC}) linear dependency on solar concentration is predictable from observations on single junction solar cells [11], the behavior of the cascade maximum power point photocurrent (J_{mpC}), and the dark current components of the top (J_{DT}) and bottom (J_{DB}) cells are not always predictable in cascade cells. The linear dependency of J_{scC} on solar concentration, shown in Figure 4.6, is a consequence of the unchanging photon flux distribution of the solar spectrum with increasing solar concentration values used in the model.

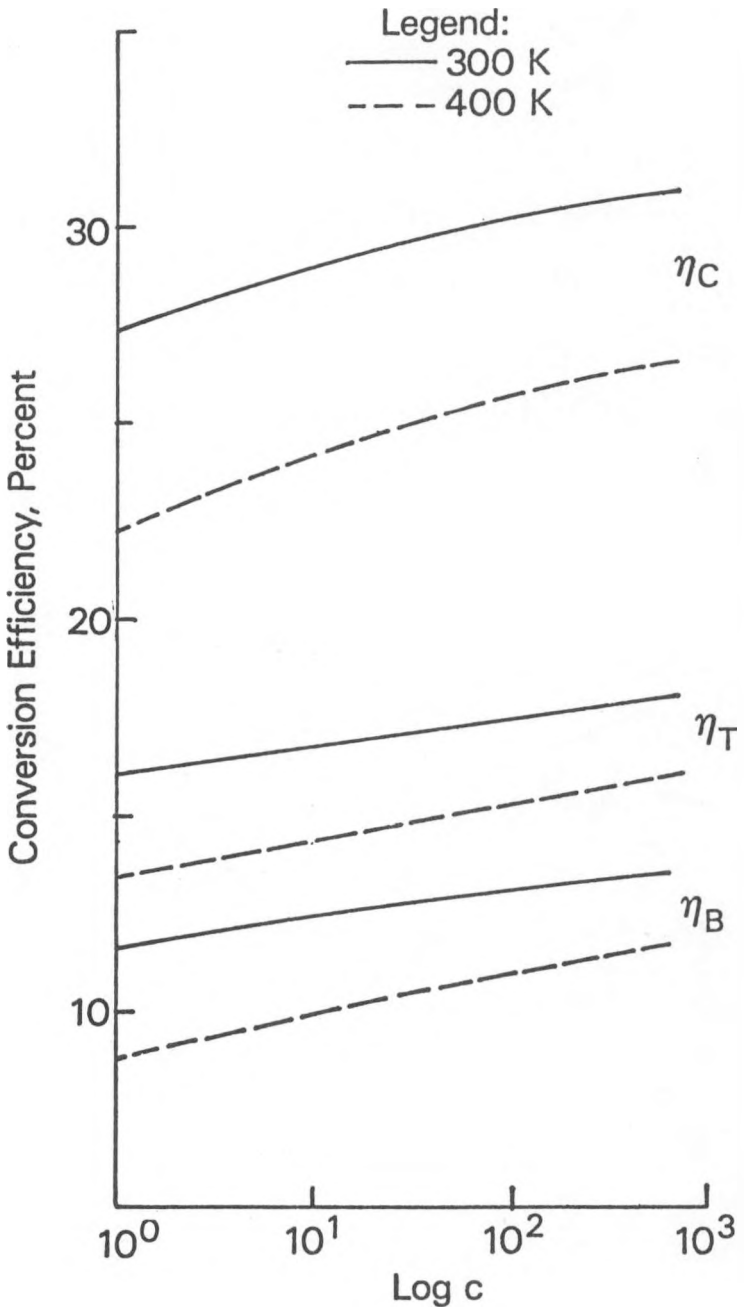

Figure 4.4 Conversion efficiency vs. solar concentration at 300 K and 400 K for the cascade and its component cells.

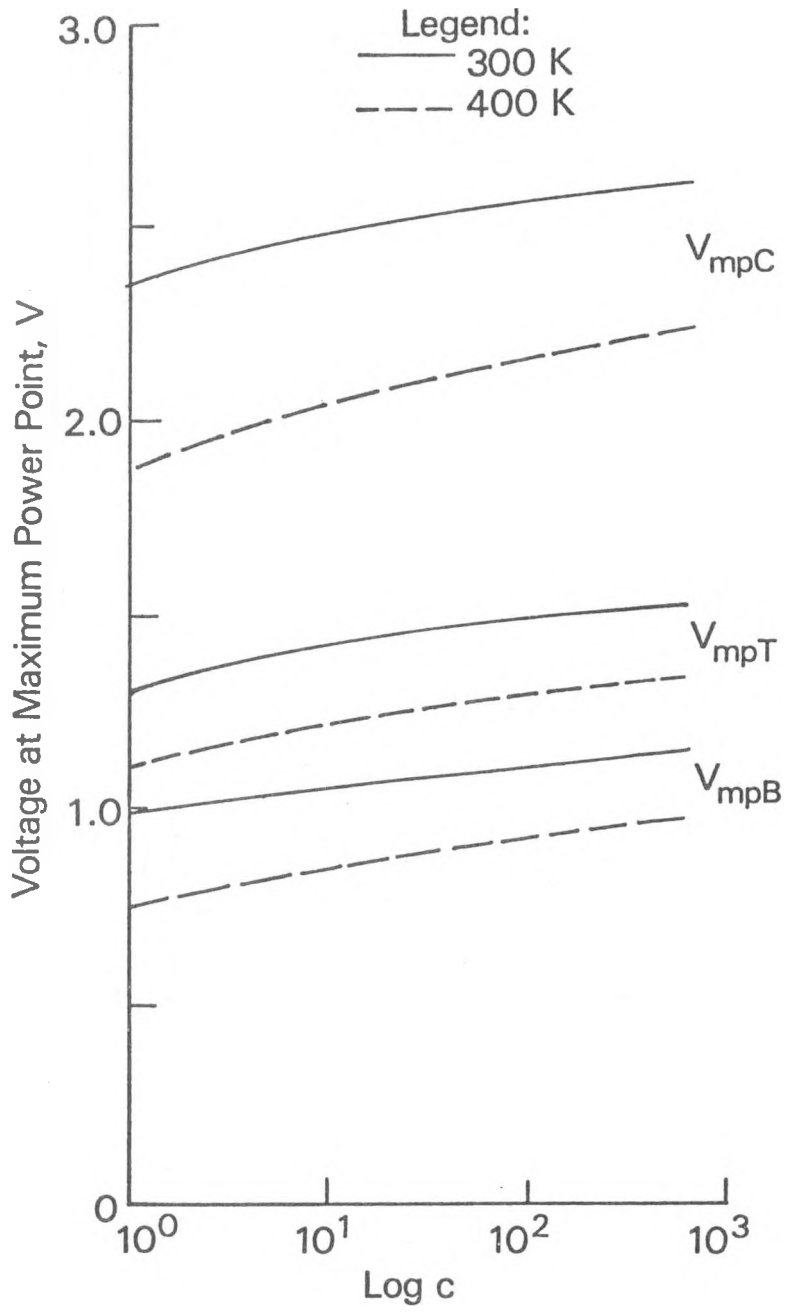

Figure 4.5 Photovoltage at the maximum power point vs. solar concentration at 300 K and 400 K for the cascade and its component cells.

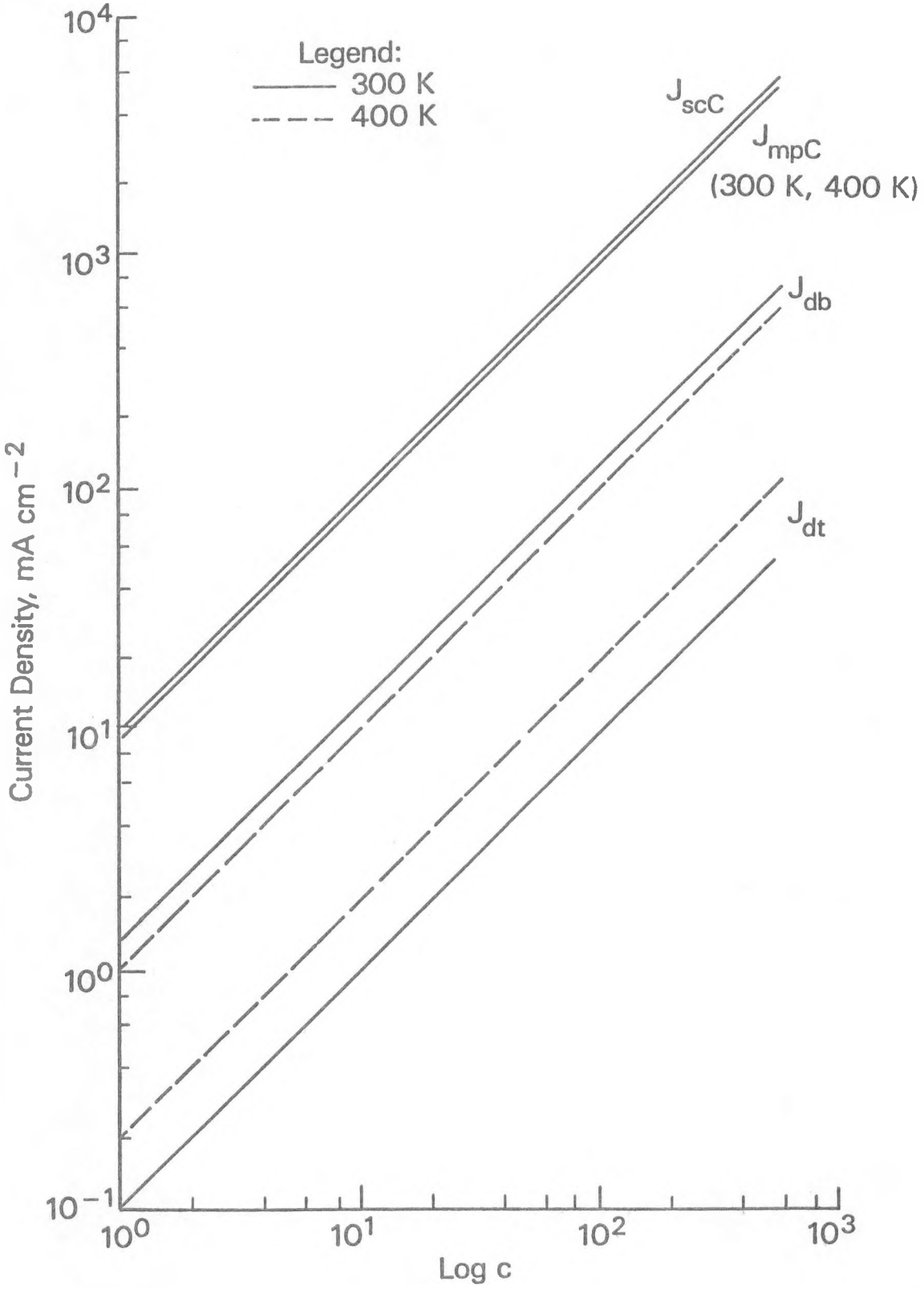

Figure 4.6 Cascade cell photocurrent, top and bottom cell current densities vs. solar concentration for 300 K and 400 K.

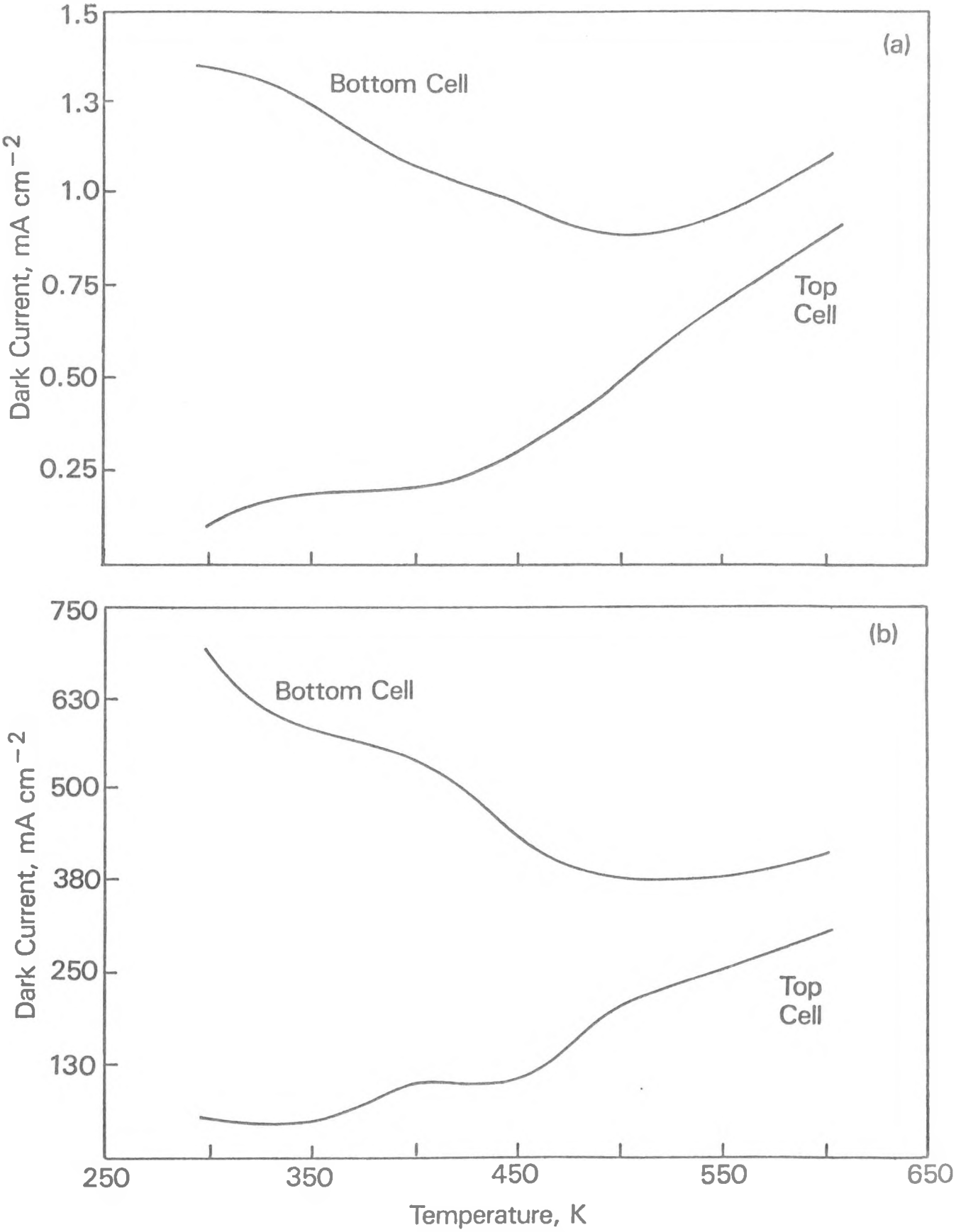

Figure 4.7 Dark current vs. temperature: a) 1 sun; b) 500 suns.

REFERENCES

1. S. M. Bedair, M. L. Timmons, J. R. Hauser, J. E. Andrews, S. B. Phatak, and M. Simons, Research on High Efficiency Cascade Solar Cells, Annual Report for the period July 1979 to June 1980, SERI Contract XM-9-8136-1, Research Triangle Institute, Research Triangle Park, NC, August 1980.

2. M. L. Timmons, S. M. Bedair, J. A. Hutchby, J. R. Hauser, and M. Simons, Development of High Efficiency Cascade Solar Cells, Annual Report for the period July 1980 to June 1981, SERI Contract XM-9-8136-1, Research Triangle Institute, Research Triangle Park, NC, July 1981.

3. M. F. Lamorte and D. H. Abbott, IEEE Trans. Electron Devices, ED-27, 4, April 1980, pp 831-40.

4. H. Kressel and J. Butler, Semiconductor Lasers and Heterojunction LED's, Academic Press, Inc., NY, 1977, p. 315.

5. S. Komiya, K. Akita, Y. Nishitani, S. Isozumi, and T. Kotani, J. Appl. Phys. 47, July 1976, p 3367.

6. R. Moon, G. Antypas, and Y. Chai, Inst. Phys. Conf. Ser. No. 45: Chapt. 1, 1979, p. 78.

7. E. Lendvay, T. Görög, and A. Tóth, J. of Cryst. Growth 53, 1981, p. 591.

8. C. Cooper, M. Ludowise, V. Aebi, and R. Moon, J. Elec. Mat. 9, 1980, p. 299.

9. M. F. Lamorte and D. H. Abbott, IEEE Trans. Electron Devices ED-27, 1980, pp. 231-49.

10. M. F. Lamorte and D. H. Abbott, Solid-State Electron. 22, 1979, pp. 467-73.

11. H. J. Hovel, Semiconductors and Semimetals: Vol. 11, Solar Cells, Academic Press, Inc., NY, 1975.

*U S GOVERNMENT PRINTING OFFICE: 1982-546-085/3297